Published in final edited form as:
Basic Res Cardiol. 2013 ; 108(3): 344. doi:10.1007/s00395-013-0344-2.

Targeted ablation of the histidine-rich Ca^{2+}-binding protein (HRC) gene is associated with abnormal SR Ca^{2+}-cycling and severe pathology under pressure-overload stress

Chang Sik Park[1,*], **Shan Chen**[2,*], **Hoyong Lee**[1,*], **Hyeseon Cha**[1], **Sunghee Hong**[1], **Peidong Han**[2], **Kenneth S. Ginsburg**[3], **Sora Jin**[1], **Inju Park**[1], **Vivek P. Singh**[2], **Hong-Sheng Wang**[2], **Clara Franzini-Armstrong**[4], **Woo Jin Park**[1], **Donald M. Bers**[3], **Evangelia G. Kranias**[2], **Chunghee Cho**[1], and **Do Han Kim**[1]

[1]School of Life Sciences and Systems Biology Research Center, Gwangju Institute of Science and Technology (GIST), Gwangju, Republic of Korea

[2]Department of Pharmacology and Cell Biophysics, University of Cincinnati College of Medicine, Cincinnati, OH

[3]Department of Pharmacology, University of California Davis, Davis, CA

[4]Department of Cell and Developmental Biology, University of Pennsylvania, Philadelphia, PA

[5]Molecular Biology Division, Center for Basic Research, Foundation for Biomedical Research of the Academy of Athens, Greece

Abstract

The histidine-rich Ca^{2+}-binding protein (HRC) is located in the lumen of the sarcoplasmic reticulum (SR) and exhibits high capacity Ca^{2+} binding properties. Overexpression of HRC in the heart resulted in impaired SR Ca^{2+} uptake and depressed relaxation through its interaction with SERCA2a. However, the functional significance of HRC in overall regulation of calcium cycling and contractility is not currently well defined. To further elucidate the role of HRC *in vivo* under physiological and pathophysiological conditions, we generated and characterized HRC-knockout (KO) mice. The KO mice were morphologically and histologically normal compared to wild type (WT) mice. At the cellular level, ablation of HRC resulted in significantly enhanced contractility, Ca^{2+} transients, and maximal SR Ca^{2+} uptake rates in the heart. However, after-contractions were developed in 50% of HRC-KO cardiomyocytes, compared to 11% in WT mice under stress conditions of high frequency stimulation (5 Hz) and isoproterenol application. A parallel examination of the electrical activity revealed significant increases in the occurrence of Ca^{2+} spontaneous SR Ca^{2+} release and delayed after depolarizations (DADs) with ISO in HRC-KO, compared to WT cells. The frequency of Ca^{2+} sparks was also significantly higher in HRC-KO cells with ISO, consistent with the elevated SR Ca^{2+} load in the KO cells. Furthermore, HRC-KO cardiomyocytes showed significantly deteriorated cell contractility and Ca^{2+}-cycling caused

Address of correspondence: Do Han Kim, College of Life Sciences, GIST, 123 Cheomdan-gwagiro, Buk-gu, Gwangju 500-712, Korea, Tel: 82-62-715-2485; dhkim@gist.ac.kr, Chunghee Cho, College of Life Sciences, GIST, Korea, Tel: 82-62-715-2490; choch@gist.ac.kr; Evangelia G. Kranias, Department of Pharmacology & Cell Biophysics, University of Cincinnati College of Medicine, 231 Albert Sabin Way, Cincinnati, OH 45267, U.S.A., Tel: 1-513-558-2377; kraniaeg@ucmail.uc.edu.
*Authors contributed equally to this work

possibly by depressed SERCA2a expression after transverse-aortic constriction (TAC). Also HRC null mice exhibited severe cardiac hypertrophy, fibrosis, pulmonary edema and decreased survival after TAC. Our results indicate that ablation of HRC is associated with poorly regulated SR Ca^{2+}-cycling, and severe pathology under pressure-overload stress, suggesting an essential role of HRC in maintaining the integrity of cardiac function.

Keywords

Calcium cycling; sarcoplasmic reticulum; hypertrophy; fibrosis; heart failure; pulmonary edema

Introduction

Heart failure is a major public health problem and about 5.7 million people in the United States have heart failure, and sudden cardiac arrest (SCA) is a leading cause of death resulting in about 325,000 deaths each year. In failing myocardium, intracellular Ca^{2+}-cycling is altered by a prolonged time course of intracellular Ca^{2+} transients, changes in systolic and diastolic Ca^{2+} levels and oxidative stress induced by increase of contraction frequency in rat cardiomyocytes [11, 16, 17, 37]. In cardiac cells, SR serves as a reservoir from which Ca^{2+} is released into the cytosol *via* the ryanodine receptor (RyR2), initiating contraction of the heart. Sequestration of Ca^{2+} from the cytosol into the SR lumen, resulting in relaxation of the heart, is mediated by sarco(endo)plasmic reticulum Ca^{2+} ATPase (SERCA2a) and its regulatory protein, phospholamban (PLN) [5]. SR Ca^{2+} storage and subsequent Ca^{2+} release are facilitated by a stable SR quaternary complex composed of RyR2, calsequestrin (CSQ), triadin (TRN) and junctin (JCN) [14, 48]. Impaired SR Ca^{2+}-cycling has been implicated in cardiac pathogenesis, underlying dilated cardiomyopathy and lethal arrhythmias [3, 8, 10, 24, 39, 42, 45]. These defects reflect altered SR Ca^{2+}-sequestration through SERCA2a or impaired SR Ca^{2+}-release through the RyR2.

The histidine-rich Ca^{2+} binding protein (HRC) has emerged as a potential regulator of both SERCA2a and RyR2 functions [4]. HRC cDNAs have been cloned from human, monkey, rabbit and mouse [18, 20, 21, 33, 36]. The HRC protein is 699–852 amino acids long in these species with a unique structural organization: a signal sequence, a histidine-rich acidic repeat region and a cysteine-rich region. While the major Ca^{2+} buffering protein in SR is CSQ, HRC, as an another Ca^{2+} buffering protein, exhibits high capacity but low affinity for Ca^{2+} [19]. Biochemical studies demonstrated that HRC binds to both TRN and SERCA2a *in vitro* in a Ca^{2+} sensitive way [2, 25]. Acute overexpression of HRC in rat neonatal or adult cardiomyocytes resulted in increased SR Ca^{2+} storage capacity and decreased Ca^{2+}-induced Ca^{2+} release from SR [9, 23]. *In vivo* cardiac overexpression of HRC resulted in delayed cytoplasmic Ca^{2+} decline and depressed cardiomyocyte SR Ca^{2+} uptake, which progressed with age to cardiac hypertrophy [12]. It is not known if the inhibitory effects of overexpressed HRC involve direct physical binding between HRC and SERCA2a or an indirect mechanism. It is also postulated that HRC may regulate SR Ca^{2+} release by interacting with TRN, which is a regulatory component of the RyR2 Ca^{2+} release complex, although no direct evidence has been shown.

Mice lacking HRC have been previously generated and it was reported that HRC ablation was mainly associated with an exaggerated response to induction of cardiac hypertrophy by isoproterenol [22]. The Ca^{2+}-cycling properties were briefly characterized using cardiac homogenates and it was reported that HRC ablation did not alter SR Ca^{2+} storage or the rates of SR Ca^{2+} uptake [22] in contrast to previous studies on overexpression of HRC. Thus, to further elucidate the functional significance of HRC in SR Ca^{2+}-cycling and its role under stress conditions, we also deleted the *Hrc* gene in the mouse and performed a detailed analysis of the cardiac phenotype of HRC-deficient mice. Our study showed that ablation of HRC resulted in increased contractile parameters and calcium kinetics in isolated cardiomyocytes associated with enhanced SR Ca^{2+} uptake rates. Interestingly, stress conditions elicited after-contractions, spontaneous SR Ca^{2+} release and delayed after depolarizations (DADs) in HRC knockout (KO) cells. Furthermore, transverse aortic constriction (TAC) in HRC-KO mice was associated with more severe cardiac hypertrophy, fibrosis, pulmonary edema and decreased survival rate compared with WTs, suggesting an important role of HRC in SR Ca^{2+}-homeostasis especially under stress conditions.

Materials and Methods

Generation of HRC deficient mice

An *Hrc* genomic clone encoding the entire *Hrc* gene was isolated from the mouse BAC library, using mouse *Hrc* complementary DNA as a probe. The targeting vector contained PGK-neo flanked by *Hrc* genomic DNA and herpes simplex virus type I thymidine kinase (HSV-tk) cassette 30, resulting in the replacement of exon 1 with the neor expression cassette in homologous recombination of 129 SvJ embryonic stem cells (Macrogen, Seoul, Korea). Subsequently, six chimaeric mice obtained from selected embryonic stem cell clones were bred to C57BL/6 mice to generate heterozygous mice. Homozygous null (*Hrc*−/−) mice were obtained by the mating of heterozygous mice. To select wild-type (WT), heterozygous and KO mice, PCR analysis of tail genomic DNA was carried out using two forward primers corresponding to the upstream common region of Exon 1 (5’-TGA GCC GGG ATG ACA CAG AAA GC- 3’), the neo^r (5’-TCG CCT TCT ATC GCC TTC TTG AC-3’) and the reverse primer corresponding to the downstream region (5’-CTT CTT CAT AGC CTT GGC GTC CA-3’). PCR was carried out, involving denaturation at 94°C for 1 minute; annealing at 60°C for 1 minute; and extension at 72°C for 3 minutes 30 seconds, for a total of 33 cycles. The genomic PCR products (2.9 and 3.6 kb) were subsequently examined in 0.7% agarose gel. 8- to 9-weeks old mice were used for the present study. All animal experiments were carried out according to the institutional guidelines for the Animal Care and Use and approved by the Animal Care and Use Committees (Institutions: GIST, University of Cincinnati and University of California Davis).

Electrophysiology of isolated left ventricular myocytes

L-type Ca^{2+} channel (dihydropyridine receptor) current or Na^+-Ca^{2+} exchanger (NCX) current was recorded in isolated ventricular myocytes with the whole-cell patch-clamp technique with an Axopatch-200B amplifier (Axon Instruments, Foster City, CA), as described previously [35, 39, 46] with some modifications. I_{Ca} was recorded in $[Ca^{2+}]_i$ buffered and in Na^+-free conditions while NCX was re corded with Ca^{2+} buffered. External

solution contained (in mM): NaCl 140, $MgCl_2$ 1, Glucose 10, HEPES 5, $CaCl_2$ 2, $BaCl_2$ 1, CsCl 4, nifedipine 0.01, ryadonine 0.005 and ouabain 0.02 (pH=7.4). Glass pipettes were filled with solution containing (in mM): aspartic acid 80, CsOH 80, TEA-Cl 20, $MgCl_2$ 2.5, HEPES 10, EGTA 11, $CaCl_2$ 7.5, CsCl 15, NaCl 10 and Na_2-ATP 4 (pH=7.2), and had a resistance of 1.5 – 2.5 M. Myocytes were depolarized from a holding potential of –55 mV to +80 mV for 100 ms via a 50 ms ramp to inactivate the Na^+ current, and were ramped down from +80 mV to −110 mV at 120 mV/sec. Once the membrane current reached steady-state, external solution was switched to one that contained 5 mM Ni^{2+}, and the NCX current was defined as the Ni^{2+}-sensitive current. Data collection and analysis were performed using pCLAMP software (Axon Instruments, Foster City, CA).

Quantitative immunoblotting

Mice were anesthetized, and hearts were excised, washed with ice-cold phosphate buffered saline (PBS), and then quickly frozen in liquid nitrogen before homogenization. To assess the levels of Ca^{2+}-cycling proteins in HRC-KO hearts, quantitative immunoblotting was performed. Polyclonal antibodies to HRC and SERCA were produced as described [12, 25]. Polyclonal antibodies to phospho-Ser16, phospho-Thr17 PLN, and phosphorylated RyR2 at serine 2809 and serine 2814 were purchased from Badrilla (Badrilla Ltd, Leeds, UK). The monoclonal anti-RyR2 antibody was from Sigma (Sigma-Aldrich Co., RBI, Natick, MA). The polyclonal anti-TRN antibody was home-made one. All the other antibodies were purchased from Affinity Bioreagents (Affinity Bioreagents Inc, Golden, CO). Protein levels were determined with AlphaEaseFC software (Alpha Innotech, San Leandro, CA).

Measurements of myocyte mechanics and Ca^{2+} kinetics

Measurements of mechanics and Ca^{2+} kinetics of isolated mouse myocytes were performed in 1.8 mM Ca^{2+}-Tyrode solution at room temperature, because acetoxymethyl ester loading at higher temperature worsens subcellular compartmentalization of the indicator and may interfere with the measurement of cytosolic Ca^{2+} concentration [34]. Cells were field stimulated at 1 Hz to steady state. As described previously [49], cell shortening and Ca^{2+} transients were measured separately in the absence or presence of isoproterenol (100 nmol/L) at 0.5 Hz. Contractility of the myocytes was examined by video edge detection. Some cells were stimulated at 5 Hz in the presence of 1 μmol/L isoproterenol at 32°C, and at 2 to 3 trains of stimulation, pacing was stopped to allow the recording of spontaneous after-contractions within 2 to 5 seconds (Figure 6). For Ca^{2+} signal measurements, cells were loaded with fura-2 (2 μM, 30 min), and Ca^{2+} transients were recorded as the 340/380 nm ratio of the resulting 510 emission at room temperature. For caffeine-induced Ca^{2+} release, the field stimulation was stopped before 10 mM caffeine was rapidly applied to the cells, and the following Ca^{2+} transients were recorded. 8–12 cells per heart were studied. In the absence of isoproterenol, 25 cells from 3 WT hearts and 32 cells from 4 KO hearts were examined for twitch Ca^{2+} transients. In the presence of isoproterenol, 21 cells from 3 WT hearts and 26 cells from 4 KO hearts were examined for twitch Ca^{2+} transients.

Cell contractility and intracellular Ca^{2+} transient measurements for the pressure overload model

The mechanical properties of ventricular myocytes were assessed using the video-based edge detection system (IonOptix), as previously described [6, 28, 29, 31] with some modifications. Briefly, laminin-coated coverslips with attached cells were placed in a chamber mounted on the stage of an inverted microscope (Nikon Eclipse TE-100F) and perfused (about 1 ml/min at 37°C) with Tyrode buffer (137 mM NaCl, 5.4 mM KCl, 1 mM $CaCl_2$, 1 mM $MgCl_2$, 10 mM glucose and 10 mM HEPES (pH 7.4)). For better observations of excitation–contraction coupling, the cells were field stimulated at a frequency of 3 Hz (30 V) using a STIM-AT stimulator/thermostat placed on a HLD-CS culture chamber/stim holder (Cell Micro Controls). Changes in cell length during shortening and relengthening were captured and analyzed using soft edge software (IonOptix). To determine changes in Ca^{2+} transient, cardiomyocytes were loaded with 0.5 μM Fura2-AM (Molecular Probes) for 15 min at 37°C. Fluorescence emission was recorded simultaneously with the contractility measurements using IonOptix. Cardiomyocytes were exposed to light emitted by a 75 W halogen lamp through either a 340 or 380 nm filter while being field-stimulated as described above. Fluorescence emission was detected between 480 and 520 nm by a photomultiplier tube after initial illumination at 340 nm for 0.5 s and then at 380 nm for the duration of the recording protocol. The 340 nm excitation scan was then repeated at the end of the protocol, and qualitative changes in the intracellular Ca^{2+} concentration were inferred from the ratio of the Fura2 fluorescence intensity at both wavelengths. To measure SR Ca^{2+} load, the stimulation was interrupted and, 5 s afterward, 20 mM of caffeine was rapidly applied to release Ca^{2+} from the stores. After intracellular Ca^{2+} concentration decline and caffeine washout, steady-state stimulation was resumed. The peak height underneath the Ca2+ transient curve during the caffeine perfusion was calculated and used as an index of the SR Ca^{2+} load. Under the sham condition, 35 cells from 4 WT hearts and 49 cells from 4 KO hearts were examined for twitch Ca^{2+} transients. Under the transverse aortic banding (TAC) condition, 52 cells form 4 WT hearts and 58 cells from 4 KO hearts were examined for twitch Ca^{2+} transients.

Oxalate-supported Ca^{2+} uptake assay

Oxalate-supported Ca^{2+} uptake measurements using cardiac homogenates were performed as described previously [27, 38] with some modification. Briefly, frozen hearts were homogenized in 50 mM potassium phosphate (pH 7.0), 10 mM NaF, 1 mM EDTA, 0.3 M sucrose, 0.3 mM PMSF, and 0.5 mM DTT. Ca^{2+} uptake rates in cardiac tissue whole homogenates (0.1 mg/ml) were measured by Millipore filtration, under conditions that restricted Ca^{2+}-uptake to SR vesicles [30]. The reaction mixture contained 20 mM MOPS (pH 7.0), 100 mM KCl, 10 mM NaN_3, 0.66 μM ruthenium red, 5 mM K-Oxalate and various concentrations of $CaCl_2$ to yield 0.01 to 10 μM free Ca^{2+}. Under these conditions, the rate of Ca^{2+} uptake is independent of luminal buffering properties and remains constant over a period of time with amplified pumping rates [32]. This is likely to differ from the pump rat e obtained for the same preparation in the absence of oxalate. Whole homogenates were incubated at 37°C for 4 minutes in the above buffer, and the reaction was initiated by the addition of Mg-ATP (final concentration, 5 mM). The rates of Ca^{2+} uptake were calculated by least squares linear regression analysis using the Ca^{2+} uptake values measure at 30, 60,

90 and 120 seconds. Values from these time points were averaged. The free Ca^{2+} concentrations in the reaction media were calculated using the "Chelator" program [43]. The results were analyzed using SigmaPlot 10 software (Systat Software Inc, Chicago, IL).

Confocal microscopy to measure Ca^{2+} sparks and spontaneous SR Ca^{2+} release

Intact cardiomyocytes were loaded with Fluo-4 AM (10 μmol/L, 15 minutes) and Ca^{2+} spark images were acquired using a Zeiss LSM 510 confocal microscope. Images were recorded with the scan line oriented along the long axis of the cell at the speed of 3.07 ms per line. The Fluo-4 AM indicator was excited at 488 nm, and emitted fluorescence was collected at >505 nm at room temperature in quiescent cells in the absence or presence of 1 μmol/L isoproterenol. Ca^{2+} sparks were analyzed with the IDL program (Research System Inc Co). In the presence of 1 μmol/L isoproterenol and after 2 trains of 5 Hz stimulation, spontaneous SR Ca^{2+} release was recorded using similar methods as Ca^{2+} sparks. Image processing and data analysis were performed using IDL program (Research Systems Inc Co). Spark identification is semi-automated. All experiments were performed at room temperature.

Induction of delayed after depolarizations in isolated cardiomyocytes

To explore whether the after contractions were associated with delayed afterdepolarizations (DADs), action potentials were recorded under current clamp mode (triggered by 2 ms just-threshold current steps) at a frequency of 5 Hz in the presence of 1 μM isoproterenol at 32°C (Figure 6c). Stimulation was paused to monitor DADs occurring within 5 sec of termination of 5-Hz stimulation, Electrodes had a resistance of 1.5–2.0 MΩ and were filled with electrode solution containing (mM): potassium aspartate 110, KCl 20, $MgCl_2$ 2.5, HEPES 10, NaCl 8, EGTA 0.05, $CaCl_2$ 0.02, Na_2-ATP 2 and Na-GTP 0.1 (pH=7.2).

Transverse aortic banding and survival rate measurement

Male mice (C57) of 9 weeks old (23–25 g) were used for the study. The animals were anesthetized with 0.3–0.5 ml of 1X Avertin solution (mixture of 2-2-2 tribromoethanol and tert-amyl alcohol) by intraperitoneal injection. Mice were ventilated with a tidal volume of 0.1 ml and a respiratory rate of 120 breaths per minute (Harvard Apparatus). A 2- to 3-mm longitudinal cut was made in the proximal portion of the sternum which allowed visualization of the aortic arch. The transverse aortic arch was ligated between the innominate and left common carotid arteries with an overlaying 27-gauge needle, and then the needle was immediately removed leaving a discrete region of constriction. The duration of TAC for WT and HRC-KO mice was 1 week and the survival rate of the animals was examined for 2 weeks. We used Gehan-Breslow analysis (Sigmastat 3.5 software) to analyze the survival rate of WT and HRC-KO mice. TAC for 1 week did not lead to heart failure, as evidenced by no negative effect on contractility in WT mice.

Histological analysis of hearts

Excised hearts were fixed in 4% formalin for 48 hours, embedded in parrafin, and sectioned (10 μm). Trichrome staining of the sectioned hearts was performed to measure the fibrotic areas. The fibrotic areas stained blue and the normal tissue stained red.

Statistical Analysis

All data are expressed as mean ± SEM. Comparison between the different groups was evaluated with the Student's *t* test or 2-way ANOVA (Student's *t* test: Figures 1, 2, 4, 5, 6 and Supplemental Figure 1, 4; 2-way ANOVA: Figures 3, 7–9 and Supplemental Figure 2, 3). Each heart was considered as a single n in Figure 1, 2, 4, 7, 8, Table 1, Supplemental Figure 2 and 3. Each cardiomyocyte was considered as a single n in Figure 3, 5, 6, 9, Supplemental and 4. Probability values (*P*) of <0.05 were considered significant.

Results

Generation of HRC-KO mice and expression levels of Ca^{2+}-cycling proteins

We disrupted the *Hrc* gene in ES cells by homologous recombination using a targeting vector in which exon 1 was replaced by a neo^r cassette (Figure 1a). Southern-blot analysis of WT (+/+) and targeted (+/−) ES cells demonstrated homologous recombination in the *Hrc* gene (Figure 1b, left). Homozygous mutant ($Hrc^{-/-}$) mice were identified by PCR analysis of genomic DNA (Figure 1b, right). Reverse transcription PCR (RT-PCR) analysis showed the lack of *Hrc* transcript (mRNA) expression in the hearts of the KO mice.

HRC-KO mice (both male and female) were viable and developed normally during at least 24 months after birth. Morphological and histological analyses indicated that hearts from the KO mice are essentially normal and hardly distinguishable from those from WT mice (Figure 1c). The heart weight to body weight ratio (HW/BW) in the KO mice was not significantly different from that of WT mice (Figure 1d). Immunoblotting analysis confirmed the lack of the HRC protein in the heart from the KO mice. The expression levels of various SR Ca^{2+}-cycling proteins such as SERCA2a, PLN, RyR2, TRN and CSQ were not changed. Unlike previous study, TRN expression was not changed in HRC KO hearts and we used mouse cardiac TRN 1 specific antibody in this study (Supplemental Figure 3). The expression levels of phosphorylated PLN and RyR were not changed as well (Figure 2).

Ca^{2+} entry

DHPR and NCX are the two major players for Ca^{2+}-entry and Ca^{2+}-removal in the cardiomyocytes. Examination of the NCX activity by whole-cell voltage clamp indicated no differences between isolated WT and HRC-KO ventricular myocytes (Supplemental Figure 1a). In addition, t here were no differences in the average current-voltage relationships of the L-type Ca^{2+} currents between WT and KO cells (Supplemental Figure 1b).

Increased contractility and Ca^{2+} transient kinetics in HRC-KO cardiomyocytes upon ISO treatment

As reported previously, *in vitro* and *in vivo* overexpression of mouse HRC impaired Ca^{2+}-cycling of the cardiomyocytes [9, 12]. In order to further elucidate the role of HRC in SR Ca^{2+}-cycling, we examined isolated cardiomyocyte mechanics and Ca^{2+} kinetics from the KO mice. Assessment of the mechanical parameters revealed significant increases in the fractional shortening by 33% (7.69 ± 0.49% in WTs vs. 10.23 ± 0.52% in KOs), rate of relaxation (+dL/dt) by 40% (106 ± 3 μm/sec in WTs vs. 149 ± 1 μm/sec in KOs), and rate of contraction (−dL/dt) by 55% (79 ± 4 μm/sec in WTs vs. 123 ± 13 μm/sec in KOs) (Figure 3a

and 3b). Fura-2 Ca^{2+} signal recording demonstrated that the baseline ratio of the fura-2 signal was not different between WT and KO cells (1.89±0. 06 in WT vs. 1.9±0.07 in KO), indicating similar diastolic Ca^{2+} levels in the cytosol. Consistent with the contractility data, analysis of the Ca^{2+} transients demonstrated that the Ca^{2+} transient amplitude (fura-2 ratio, 340/380 nm), measured by peak changes from baseline, was increased by 30% in HRC-KO myocytes (0.41 ± 0.04 in WTs vs. 0.54 ± 0.02 in KO s), and the time constant of Ca^{2+} transient decay ( ) was abbreviated by 22%, compared to WTs (0. 66 ± 0.03 sec in WTs vs. 0.51 ± 0.03 sec in KOs) (Figure 3c and 3d). However, the amplitude of caffeine-induced Ca^{2+} release did not change (0.96 ± 0.06 in WTs vs. 1.02 ± 0.05 in KO s), indicating similar SR Ca^{2+} load levels between HRC-KO and WT cells (Figure 3d). These results demonstrated that the fractional release of SR Ca^{2+} was significantly increased in HRC-KO cells compared to the WTs.

To examine the effects of β-adrenergic agonists, isolated cardiomyocytes were subjected to 1 00 nmol/L isoproterenol stimulation, and the contractile parameters and Ca^{2+} kinetics were evaluated. Isoproterenol stimulation was associated with significant increases in contractile parameters and Ca^{2+} transient kinetics in both WT and HRC-KO myocytes (Figure 3). Although the Ca^{2+} transient amplitude was higher by 19% in the KO myocytes compared to WTs (1.19 ± 0.12 in WTs vs. 1.40 ± 0. 03 in KOs), and the time constant of Ca^{2+} transient decay was abbreviated by 20% (0.32 ± 0.02 in WTs vs. 0.25 ± 0.02 in KOs), the maximally stimulated contractile parameters were similar between the two groups. There are two simple possibilities to explain the results. First, ISO could lead to inducing maximal contractility in both types of samples. Second, the relative increase in Ca^{2+} transients upon ISO addition is less in the KO animals, which could translate into less enhanced contraction. The relationship between contraction and $[Ca^{2+}]_i$ is highly non-linear and that ISO decreases myofilament Ca^{2+} sensitivity. Importantly, the amplitude of caffeine-induced Ca^{2+} release was higher by 26% in HRC-KO cells compared to WTs after the application of isoproterenol (1.31 ± 0. 05 in WTs vs. 1.63 ± 0.08 in KOs) indicating an elevated SR Ca^{2+} load (Figure 3d).

SR Ca^{2+} uptake

Our findings on the changes in Ca^{2+} transient kinetics in hearts lacking HRC imply an alteration in the SR Ca^{2+} transport system of the KO hearts. Indeed, a previous study showed that SR Ca^{2+} uptake was significantly inhibited in mouse hearts overexpressing HRC [12]. Thus, we examined the effects of HRC deficiency on the regulation of the Ca^{2+}-dependence of SR Ca^{2+} uptake to further evaluate the underlying subcellular mechanisms. We measured Ca^{2+} uptake in the presence of 5 mM oxalate. We found that the maximal rates of Ca^{2+} uptake were significantly higher in HRC-KO than WT hearts (65.6 ± 2.1 vs. 54.8 ± 1.4 nmol/mg/min, $p<0.001$) (Figure 4). On the other hand, the concentration of Ca^{2+} for half maximal activation of Ca^{2+} uptake (EC_{50}) was similar between WT and HRC-KO hearts (6.34 ± 0.05 vs. 6.23 ± 0.11 nmole/mg/min). Importantly, the increased Vmax is not due to increased SERCA expression (Figure 2) indicating a potential regulatory effect of HRC on Vmax. Thus, HRC regulates the V_{max} of SR Ca^{2+} uptake and not its Ca^{2+}-affinity. Direct interaction of HRC with SERCA2a, previously shown to occur *in vitro* [23], might be responsible for the regulation of SERCA2a by HRC. Additionally, our electron micrograph

results showed that the SR volume relative to the fiber volume was not significantly different, although the overall SR surface area per fiber volume was increased slightly (refer to Figure 5 and the legend). Taken together, HRC ablation increased the maximal rates of SR Ca^{2+} uptake without any change in SR volume.

Stress-induced after-contractions, spontaneous SR Ca^{2+} release and DADs in HRC-KO cardiomyocytes

To determine the effects of stress conditions in HRC-deficient cells, HRC-KO and WT cardiomyocytes were subjected to 2 to 3 trains of 5-Hz field stimulation in the presence of 1 μmol/L isoproterenol. Spontaneous after-contractions occurred in 50% of HRC-KO cells within 5 seconds after pacing was stopped, compared with 11% of WT cells (Figure 6a). Consistent with the increase in after-contractions, further assessment of the Ca^{2+} transients at 5-Hz plus 1μmol/L isoproterenol stimulation demonstrated that 73% of the HRC-KO cells developed Ca^{2+} spontaneous SR Ca^{2+} release, whereas only 11% of the WT cells exhibited abnormal Ca^{2+} transients after the electrical stimulation was stopped (Figure 6b). In myocytes stimulated at 5 Hz (and 32°C), isoproterenol (1 μmol/L) induced delayed afterdepolarizations (DADs) in 82% of the HRC-KO myocytes compared with only 7% of WT myocytes (Figure 6c). Thus, the HRC-KO myocytes exhibit SR Ca release events that are pro-arrhythmic.

Ca^{2+} sparks in HRC-KO myocytes

One of the potential mechanisms underlying the increased probability of spontaneous after-contractions (Acs) and spontaneous SR Ca^{2+} release occurring in HRC-KO animals in the presence of ISO (Figures 6a and 6b) is SR Ca^{2+} leak either due to SR Ca^{2+} overload [8, 32, 42] and/or defects in RyR2 Ca^{2+} release [44]. The SR Ca^{2+} leak can be examined by measuring Ca^{2+} sparks which represent the coordinated opening of RyR2s *in situ.* We examined the Ca^{2+} spark proper ties with (Figure 6d) or without 1 μmol/L isoproterenol stimulation (Supplemental Figure 4) in intact quiescent cells. The spark frequency and the fractional SR Ca^{2+} release were significantly increased in HRC-KO cardiomyocytes with respect to WTs at the basal condition (Supplemental Figure 4), although there was no difference in SR Ca^{2+} content between WT and HRC-KO cardiomyocytes (Figure 3d), indicating a direct effect of HRC-KO on RyR2 function. No differences in amplitude, full-width-at-half-maximal amplitude (FWHM) and full-duration-at-half-maximal amplitude (FDHM) were detected between WT and HRC-KO cells (Supplemental Figure 4). Also the spark frequency was significantly increased by 40% in HRC-KO cardiomyocytes with respect to WTs after 1 μmol/L isoproterenol was applied (Figure 6d). Spark amplitude, FWHM and FDHM were not changed by isoproterenol. This indicated that under stress conditions, HRC-KO cardiomyocytes are more likely to exhibit SR Ca^{2+} leak than WT cells, which may increase the incidence of Acs, spontaneous SR Ca^{2+} release and DADs in HRC-KO cells.

Exacerbated response of HRC-KO mice to pressure-overload

We examined the hypertrophic response in WT and HRC-KO mice using a pressure-overload model of cardiac hypertrophy. Transverse aortic constriction (TAC) resulted in a

23% increase in HW/BW (Figure 7a) and a 40% increase in the heart weight to tibia length ratio (HW/TL) (Figure 7b) in WT mice after 1 week. This hypertrophic growth was exacerbated significantly in HRC-KO mice, because there was a 52% increase in HW/BW and a 70% increase in HW/TL at 1 week after TAC. Echocardiographic analysis revealed a 37% decrease in heart function (shown as fractional shortening (FS)) and more severe cardiac hypertrophy in TAC operated HRC-KO mice, compared with WT TAC mice (refer to the parameters shown in Table 1). Microscopic analysis of histological ventricular cross-sections revealed that the fibrotic area was significantly increased in HRC-KO mice compared with WT mice after TAC operation (Figure 7c and 7d).

We also examined the possible symptoms of congestive heart failure in pressure over-loaded hearts from WT and HRC-KO mice by measuring the ratio of lung weight (LW)/TL (Figure 8a and 8b). TAC-1 week resulted in a 20% increase in HW/BW and a 30% increase in HW/TL in WT mice, but a 50% increase in HW/BW and a 69% increase in HW/TL in HRC-KO mice. The lungs from HRC-KO mice were obviously discolored (Figure 8a) and LW/TL was significantly increased (Figure 8b) in HRC-KO animals (42%), compared with WT TAC mice, indicating that severe pulmonary edema occurred in HRC-KO TAC mice. Furthermore, the survival rate of HRC-KO mice was significantly decreased after TAC operation (Figure 8c) probably due to irregular Ca^{2+}-cycling, pulmonary edema and cardiac fibrosis leading to reduced cardiac function. These results suggest that HRC-KO mice show exacerbated response to pressure overload and accelerated transition of hypertrophy to heart failure.

Decreased cardiac contractility and Ca^{2+} transient kinetics in pressure over-loaded HRC-KO mice

The exacerbated response of HRC-KO mice to pressure-overload was further evaluated by measuring contractile parameters and Ca^{2+} kinetics using the WT and HRC-KO animals (Figure 9). Assessment of the mechanical parameters in the sham group revealed significant increases in the fractional shortening by 32% (7.4 ± 0.3% in WT sham vs. 9.7 ± 0.3% in KO sham), rate of relaxation (+dL/dt) by 36% (70.18 ± 7.07 μm/sec in WT sham vs. 95.71 ± 13.52 μm/sec in KO sham), and rate of contraction (–dL/dt) by 33% (103.34 ± 10.71 μm/sec in WT sham vs. 137.88 ± 17.99 μm/sec in KO sham) (Figure 9a and 9b).

Fura-2 Ca^{2+} signal recording demonstrated that the resting fura-2 ratio was not significantly increased in KO vs. WT cells (1.08 ± 0.06 in WT sham vs. 1.11 ± 0.10 in KO sham, p = 0.073). Consistent with the contractility data, analysis of the Ca^{2+} transients in the sham group demonstrated that the Ca^{2+} transient amplitude (fura-2 ratio, 340/380 nm) was increased by 52% in HRC-KO sham cells (0.21 ± 0.01 in WT sham vs. 0.32 ± 0.01 in KO sham), and the time required to reach 50% of baseline (T_{50}) was shortened by 19% in HRC-KO sham cells (0.26 ± 0.003 sec in WT sham vs. 0.21 ± 0.004 sec in KO sham) (Figure 9c and 9d). However, there was no change in SR Ca^{2+} load between WT sham and HRC-KO sham cells (0.54 ± 0.03 in WT sham vs. 0.59 ± 0.03 in KO sham) (Figure 9d), indicating that the fractional release of SR Ca^{2+} was significantly increased in HRC-KO sham cells compared to WT sham cells.

However, 1 week TAC was associated with significantly deteriorated contractile parameters and Ca^{2+} transient kinetics in HRC-KO myocytes (Figure 9). Analysis of the mechanical parameters in TAC group revealed significant decreases in the fractional shortening by 24% (6.86 ± 0.28% in WT TAC vs. 5.2 ± 0.16% in KO TAC), rate of relaxation (+dL/dt) by 50% (67.76 ± 12.29 μm/sec in WT TAC vs. 33.89 ± 4.88 μm/sec in KO TAC), and rate of contraction (–dL/dt) by 49% (96.12 ± 15.84 μm/sec in WT TAC vs. 49.15 ± 6.4 μm/sec in KO TAC) (Figure 9a and 9b).

Fura-2 Ca^{2+} signal recording in TAC group demonstrated that the baseline ratio of the fura-2 signal was significantly increased in KO TAC cells (1.06 ± 0.05 in WT TAC vs. 1.14 ± 0.04 in KO TAC). Consistent with the contractility data, analysis of Ca^{2+} transients in TAC group demonstrated that the Ca^{2+} transient amplitude (fura-2 ratio, 340/380 nm) was decreased by 47% in HRC-KO TAC cells (0.19 ± 0.009 in WT TAC vs. 0.1 ± 0.007 in KO TAC), and the time required to reach 50% of baseline (T_{50}) was prolonged by 16% in HRC-KO TAC cells (0.25 ± 0.001 sec in WT TAC vs. 0.29 ± 0.003 sec in KO TAC) (Figure 9c and 9d). The amplitude of caffeine-induced Ca^{2+} release was also decreased by 37% (0.49 ± 0.02 in WT TAC vs. 0.31 ± 0.017 in KO TAC) (Figure 9c and 9d) and the expression of SERCA2a was reduced by 63% in HRC-KO TAC hearts compared with WT TAC hearts (Supplemental Figure 2), indicating the impaired Ca^{2+}-cycling caused by the reduced SERCA2a expression after TAC.

Discussion

This study reports for the first time that HRC ablation is associated with increased contractility and Ca^{2+}-cycling properties under basal conditions in cardiomyocytes but impairs Ca^{2+}-cycling resulting in detrimental effects under stress conditions. One possible explanation for the stimulatory effects under basal conditions is that HRC has an inhibitory interaction with SERCA2a [2, 12] and that this inhibitory effect of HRC on SR Ca^{2+} uptake is relieved in HRC deficient cells, resulting in faster SR Ca^{2+} uptake. HRC also binds to TRN, which may serve as an inhibitor for RyR2 and may thus inhibit SR Ca^{2+} release [2, 13, 41], consistent with our observations showing the higher fractional Ca^{2+} release from the SR (Figure 3d and 9d) and enhanced Ca^{2+} spark frequency in HRC-KO mice (Figure 6d and Supplemental Figure 4) I_{Ca} and SR Ca^{2+} load were unaltered (Supplemental Figure 1a and Figure 3d) by HRC-KO, but fractional SR Ca^{2+} release was enhanced resulting in enhanced Ca^{2+} transients and myocyte contractions. This reflects increased RyR2 sensitivity in HRC-KO myocytes during E-C coupling,. Upon isoproterenol stimulation the combination of enhanced SR Ca^{2+} uptake and RyR2 sensitivity in the HRC-KO resulted in increased SR Ca^{2+} load (vs. WT) and profoundly enhanced Ca^{2+} spark frequency and the propensity for arrhythmogenic spontaneous SR Ca^{2+} release, after-contractions and DADs (Figure 6). Thus, normal HRC expression levels stabilize SR Ca^{2+}-cycling, and ablation of HRC ma y increase susceptibility to cardiac arrhythmias.

Alteration of Ca^{2+}-cycling in HRC-KO mice

A previous study in another HRC-KO mouse model did not detect significant Ca^{2+}-cycling alterations, unlike our present findings. However, Jaehnig *et al.* did not perform any

myocyte $[Ca^{2+}]_i$ measurements. In cardiac microsomal vesicles they found no significant alteration in $[^3H]$ ryanodine binding or in Ca^{2+} uptake at 50 μM $[Ca^{2+}]_i$ in WT vs. HRC-KO (48 ± 8 and 65 ± 12 nmol/mg, respectively). Although not significant, their higher mean Ca^{2+} uptake value is in the same direction as our 20% increase in V_{max} of SR Ca^{2+} uptake and 22% increase in rate of twitch $[Ca^{2+}]_i$ decline. We further found that HRC-KO myocytes were more susceptible to isoproterenol-induced SR Ca^{2+} overload, after-contraction and spontaneous SR Ca^{2+} release. We also found that HRC-KO myocytes presented more deteriorated Ca^{2+}-cycling, SR Ca^{2+} load and cell contractility under pressure over-load condition (Figure 9), and were susceptible to cardiac hypertrophy (Figure 7) consistent with the observation by Jaehnig *et al*. that HRC ablation exacerbated isoproterenol-induced cardiac hypertrophy. So, in broad strokes these two HRC-KO models produced compatible results, but we have more extensively characterized myocyte Ca^{2+}-cycling and pressure-overload induced hypertrophy.

Increased fractional SR Ca^{2+} release under basal condition

With ISO, SR Ca^{2+} content was higher in HRC-KO myocytes (Figure 3d), and we suspect that this is because ISO amplifies the SERCA2a enhancement in HRC-KO myocytes, but it did not further enhance RyR2 function. We have shown before that ISO does not enhance fractional SR Ca^{2+} release [11]. Overall ISO increased fractional SR Ca^{2+} release for both WT and HRC-KO, but the percentage was smaller for the HRC-KO animal.

Increased SR Ca^{2+} uptake rates in HRC-KO cardiomyocytes

The increased V_{max} of SR Ca^{2+} s in HRC-KO cardiomyocytes (based on both oxalate supported SR Ca^{2+} uptake and rate of twitch $[Ca^{2+}]_i$ decline) mirrors a previous study with HRC overexpression in cardiac myocytes [11], where twitch $[Ca^{2+}]_i$ decline was slowed and V_{max} for SR Ca^{2+} uptake was inhibited in mice overexpressing HRC. Because the $[Ca^{2+}]_i$ for half maximal activation of Ca^{2+} uptake was similar between WT and HRC-KO, the increased Ca^{2+} uptake rate appears to be predominantly an increase in V_{max} rather than altered Ca^{2+} binding affinity of SERCA2a. HRC might regulate the V_{max} of SERCA2a via a direct interaction with SERCA2a [2]. The level of SR Ca^{2+} load was found unaltered in the absence of HRC under basal conditions, despite the increased Ca^{2+} uptake rates. That might be due to the absence of a SR Ca^{2+} buffering protein, HRC (CSQ level unchanged, Figure 2). Alternatively, the higher fractional SR Ca^{2+}-release and Ca^{2+} transient amplitude would enhance extrusion of Ca^{2+} via the NCX to limit net increase of SR Ca^{2+} load in HRC-KO cells. The structure and volume of the SR, determined by an electron microscopic, were also not significantly different between HRC-WT and -KO mice (Figure 5). However, isoproterenol stimulation drove HRC-KO cardiomyocytes to be Ca^{2+}-overloaded in the SR, compared to the WTs (Figure 3d), possibly due to further activation of Ca^{2+} uptake by phosphorylation of PLN.

Increased potential for arrhythmogenesis under stress condition in HRC-KO mice

Notably, the HRC-KO myocytes exhibit increased Ca^{2+} sparks, after-contractions, spontaneous SR Ca^{2+} release and DADs under stress. DADs are usually associated with fast pacing, and are the result of SR Ca^{2+} overload and SR Ca^{2+} leak [8, 42, 47]. Stress with 5

Hz stimulation plus 1 μmol/L isoproterenol increased the SR Ca^{2+} load to higher levels in HRC-KO cardiomyocytes compared to WTs, due to increased SERCA2a activity (Figure 4). The higher SR Ca^{2+} load may lead to spontaneous SR Ca^{2+} release (SR Ca^{2+} leak) or Ca^{2+} sparks in the KO myocytes, shown as increased frequencies of spontaneous SR Ca^{2+} release (Figure 6b), DADs and triggered action potentials (Figure 6c). Thus, the resulting elevation of $[Ca^{2+}]_i$ activates inward NCX current, which extrudes Ca^{2+} from the cell in exchange for Na^+. This inward NCX current drives depolarization towards the threshold for a triggered AP [27]. Ablation of PLN resulted in enhanced SERCA2 Ca^{2+} uptake, increased SR Ca^{2+} content, augmented SR Ca^{2+} transient amplitude and accelerated Ca^{2+}-cycling properties [27], without any observed arrhythmias. However, the HRC-KO mouse model differs from the PLN-KO model, since HRC does not only affect SERCA2 activity, but also binds and interacts with TRN, in a Ca^{2+} sensitive manner [2]. A recent study on TRN demonstrated that overexpression of TRN disrupts structural and functional integrity of the cardiac Ca^{2+} release unit, leading to ventricular arrhythmias [7, 41]. HRC is similar to CSQ in aspects of Ca^{2+} buffering properties and its interaction with TRN. A previous study indicated that CSQ2 acts as a SR luminal Ca^{2+} sensor, modulating RyR2 function through CSQ2-TRN (JCN) and TRN (JCN)-RyR2 interactions [12]. Furthermore, a CSQ2 mutant, with no capacity for Ca^{2+} binding, was found to be associated with catecholamine-induced polymorphic ventricular tachycardia (CPVT) [40]. Thus, it is possible that in addition to enhancing SR Ca^{2+} uptake rate, HRC-KO sensitizes RyR2, thereby amplifying the arrhythmogenic potential of isoproterenol-induced enhancement of SR Ca^{2+}-cycling. The SERCA effect of HRC-KO seems to be dominant over the RyR2 effect, because there was a net increase in SR Ca^{2+} load in the KO vs. WT (whereas a dominant RyR2 effect would have lowered SR Ca^{2+} load).

Severe cardiac hypertrophy, pulmonary edema and fibrosis in HRC-KO

According to previous reports, the expression levels of HRC are significantly decreased in human and mouse models of heart failure [12] and overexpression of HRC protects against ischemia/reperfusion-induced cardiac injury [50]. Thus, it is likely that the expression level of HRC is closely associated with the pathological state of the heart. The more severe cardiac fibrosis, pulmonary edema, and decreased survival rate in HRC-KO animals (Figure 7 and 8) could be mediated 7 by CaMKII-mediated Ca^{2+} signaling [26]. Recently, a human HRC polymorphism was found to be associated with cardiac arrhythmias in DCM patients [1], suggesting that abnormal HRC behavior may have detrimental effects under stress or pathophysiological conditions. In fact, Figure 7 and 8 shows that in response to pressure-overload, HRC-KO animals develop not only more severe cardiac hypertrophy, worse cardiac function and severe cardiac fibrosis, but also severe pulmonary edema and decreased survival rate, as compared with WTs. Furthermore pressure over-load in HRC-KO mice presented significantly increased $[Ca^{2+}]_i$, reduced cardiomyocyte contractility and Ca^{2+}-cycling (Figure 9) caused by decreased expression of SERCA2a (Supplemental Figure 2), suggesting symptom of heart failure in HRC-KO TAC animal [15].

In conclusion, our findings revealed that ablation of HRC is associated with enhanced contractility, SR Ca^{2+}-cycling properties and maximal SR Ca^{2+} uptake rates in cardiomyocytes. HRC-KO cardiomyocytes were found to show a significant increase in the

after-contractions, spontaneous SR Ca^{2+} release and DADs under stress conditions. Furthermore, HRC-KO mice showed cardiac dysfunction, fibrosis and pulmonary edema at 1 week after TAC. Thus, our results provide evidence that HRC is required for maintaining proper SR Ca^{2+}-cycling, potentially through interactions with SERCA2a and TRN, and proper cardiac function. HRC could be a good target for heart failure, and maintenance of HRC expression may prevent heart failure progression and cardiac arrhythmias.

Supplementary Material

Refer to Web version on PubMed Central for supplementary material.

Acknowledgments

This work was supported by Korean Systems Biology Research Grant M10503010001-06N0301-00110 (to D.H.K. and C.C.); GIST Systems Biology Infrastructure Establishment Grant (to D.H.K. and C.C.); National Institutes of Health Grants HL-48093 (to C.F.A), HL-26507 (to E.G.K.), HL-64018 and HL-77101 (to E.G.K.).

References

1. Arvanitis DA, Sanoudou D, Kolokathis F, Vafiadaki E, Papalouka V, Kontrogianni-Konstantopoulos A, Theodorakis GN, Paraskevaidis IA, Adamopoulos S, Dorn GW 2nd, Kremastinos DT, Kranias EG. The Ser96Ala variant in histidine-rich calcium-binding protein is associated with life-threatening ventricular arrhythmias in idiopathic dilated cardiomyopathy. Eur Heart J. 2008; 29:2514–2525. [PubMed: 18617481]
2. Arvanitis DA, Vafiadaki E, Fan GC, Mitton BA, Gregory KN, Del Monte F, Kontrogianni-Konstantopoulos A, Sanoudou D, Kranias EG. Histidine-rich Ca^{2+}-binding protein interacts with sarcoplasmic reticulum Ca^{2+}-ATPase. Am J Physiol Heart Circ Physiol. 2007; 293:H1581–H1589. [PubMed: 17526652]
3. Bers DM. Calcium cycling and signaling in cardiac myocytes. Annu Rev Physiol. 2008; 70:23–49. [PubMed: 17988210]
4. Bers DM, Guo T. Calcium signaling in cardiac ventricular myocytes. Ann N Y Acad Sci. 2005; 1047:86–98. [PubMed: 16093487]
5. Brittsan AG, Kranias EG. Phospholamban and cardiac contractile function. J Mol Cell Cardiol. 2000; 32:2131–2139. [PubMed: 11112989]
6. Cha H, Kim JM, Oh JG, Jeong MH, Park CS, Park J, Jeong HJ, Park BK, Lee YH, Jeong D, Yang DK, Bernecker OY, Kim DH, Hajjar RJ, Park WJ. PICOT is a critical regulator of cardiac hypertrophy and cardiomyocyte contractility. J Mol Cell Cardiol. 2008; 45(6):796–803. [PubMed: 18929570]
7. Chopra N, Yang T, Asghari P, Moore ED, Huke S, Akin B, Cattolica RA, Perez CF, Hlaing T, Knollmann-Ritschel BE, Jones LR, Pessah IN, Allen PD. Ablation of triadin causes loss of cardiac Ca^{2+} release units, impaired excitation-contraction coupling, and cardiac arrhythmias. Proc Natl Acad Sci U S A. 2009; 106:7636–7641. [PubMed: 19383796]
8. Elliott EB, Hasumi H, Otani N, Matsuda T, Matsuda R, Kaneko N, Smith GL, Loughrey CM. K201 (JTV-519) alters the spatiotemporal properties of diastolic Ca^{2+} release and the associated diastolic contraction during β-adrenergic stimulation in rat ventricular cardiomyocytes. Basic Res Cardiol. 2011; 106:1009–1022. [PubMed: 21901290]
9. Fan GC, Gregory KN, Zhao W, Park WJ, Kranias EG. Regulation of myocardial function by histidine-rich, calcium-binding protein. Am J Physiol Heart Circ Physiol. 2004; 287:H1705–H1711. [PubMed: 15191886]
10. Florea S, Anjak A, Cai WF, Qian J, Vafiadaki E, Figueria S, Haghighi K, Rubinstein J, Lorenz J, Kranias EG. Constitutive phosphorylation of inhibitor-1 at Ser67 and Thr75 depresses calcium cycling in cardiomyocytes and leads to remodeling upon aging. Basic Res Cardiol. 2012; 107:279. [PubMed: 22777184]

11. Ginsburg KS, Bers DM. Modulation of excitation-contraction coupling by isoproterenol in cardiomyocytes with controlled SR Ca^{2+} load and I_{Ca} trigger. J. Physiol. 2004; 556:463–480. [PubMed: 14724205]
12. Gregory KN, Ginsburg KS, Bodi I, Hahn H, Marreez YM, Song Q, Padmanabhan PA, Mitton BA, Waggoner JR, Del Monte F, Park WJ, Dorn GW 2nd, Bers DM, Kranias EG. Histidine-rich Ca^{2+} binding protein: a regulator of sarcoplasmic reticulum calcium sequestration and cardiac function. J Mol Cell Cardiol. 2006; 40:653–665. [PubMed: 16600288]
13. Györke I, Hester N, Jones LR, Györke S. The role of calsequestrin, triadin, and junctin in conferring cardiac ryanodine receptor responsiveness to luminal calcium. Biophys J. 2004; 86(4): 2121–2128. [PubMed: 15041652]
14. Györke S, Terentyev D. Modulation of ryanodine receptor by luminal calcium and accessory proteins in health and cardiac disease. Cardiovasc Res. 2008; 77:245–255. [PubMed: 18006456]
15. Hasenfuss G. Alterations of calcium-regulatory proteins in heart failure. Cardiovasc Res. 1998; 37:279–289. [PubMed: 9614485]
16. Heinzel FR, Luo Y, Dodoni G, Boengler K, Petrat F, Di Lisa F, de Groot H, Schulz R, Heusch G. Formation of reactive oxygen species at increased contraction frequency in rat cardiomyocytes. Cardiovasc Res. 2006; 71(2):374–382. [PubMed: 16780821]
17. Heusch G. Heart rate and heart failure. Circ J. 2011; 75:229–236. [PubMed: 21041970]
18. Hofmann SL, Brown MS, Lee E, Pathak RK, Anderson RG, Goldstein JL. Purification of a sarcoplasmic reticulum protein that binds Ca^{2+} and plasma lipoproteins. J Biol Chem. 1989; 264:8260–8270. [PubMed: 2498310]
19. Hofmann SL, Goldstein JL, Orth K, Moomaw CR, Slaughter CA, Brown MS. Molecular cloning of a histidine-rich Ca^{2+}-binding protein of sarcoplasmic reticulum that contains highly conserved repeated elements. J Biol Chem. 1989; 264:18083–18090. [PubMed: 2808365]
20. Hofmann SL, Topham M, Hsieh CL, Francke U. cDNA and genomic cloning of HRC, a human sarcoplasmic reticulum protein, and localization of the gene to human chromosome 19 and mouse chromosome 7. Genomics. 1991; 9:656–669. [PubMed: 2037293]
21. Hong S, Kim TW, Choi I, Woo JM, Oh J, Park WJ, Kim DH, Cho C. Complementary DNA cloning, genomic characterization and expression analysis of a mammalian gene encoding histidine-rich calcium binding protein. Biochim Biophys Acta. 2005; 1727:188–196. [PubMed: 15777620]
22. Jaehnig EJ, Heidt AB, Greene SB, Cornelissen I, Black BL. Increased susceptibility to isoproterenol-induced cardiac hypertrophy and impaired weight gain in mice lacking the histidine-rich calcium-binding protein. Mol Cell Biol. 2006; 26:9315–9326. [PubMed: 17030629]
23. Kim E, Shin DW, Hong CS, Jeong D, Kim DH, Park WJ. Increased Ca^{2+} storage capacity in the sarcoplasmic reticulum by overexpression of HRC (histidine-rich Ca2+ binding protein). Biochem Biophys Res Commun. 2003; 300:192–196. [PubMed: 12480542]
24. Kranias EG, Bers DM. Calcium and cardiomyopathies. Subcell Biochem. 2007; 45:523–537. [PubMed: 18193651]
25. Lee HG, Kang H, Kim DH, Park WJ. Interaction of HRC (histidine-rich Ca^{2+}-binding protein) and triadin in the lumen of sarcoplasmic reticulum. J Biol Chem. 2001; 276:39533–39538. [PubMed: 11504710]
26. Ling H, Zhang T, Pereira L, Means CK, Cheng H, Gu Y, Dalton ND, Peterson KL, Chen J, Bers DM, Brown JH. Requirement for Ca^{2+}/calmodulin-dependent kinase II in the transition from pressure overload-induced cardiac hypertrophy to heart failure in mice. J Clin Invest. 2009; 119:1230–1240. [PubMed: 19381018]
27. Luo W, Grupp IL, Harrer J, Ponniah S, Grupp G, Duffy JJ, Doetschman T, Kranias EG. Targeted ablation of the phospholamban gene is associated with markedly enhanced myocardial contractility and loss of beta-agonist stimulation. Circ Res. 1994; 75:401–409. [PubMed: 8062415]
28. Oh JG, Jeong D, Cha H, Kim JM, Lifirsu E, Kim J, Yang DK, Park CS, Kho C, Park S, Yoo YJ, Kim DH, Kim J, Hajjar RJ and Park WJ. PICOT increases cardiac contractility by inhibiting PKCζ activity. J Mol Cell Cardiol. 2012; 53(1):53–63. [PubMed: 22449794]

29. Oh JG, Kim J, Jang SP, Nguen M, Yang DK, Jeong D, Park ZY, Park SG, Hajjar RJ and Park WJ. Decoy peptides targeted to protein phosphatase 1 inhibit dephosphorylation of phospholamban in cardiomyocytes. J Mol Cell Cardiol. 2013; 56:63–71. [PubMed: 23262438]
30. Pagani ED, Solaro RJ. Coordination of cardiac myofibrillar and sarcotubular activities in rats exercised by swimming. Am J Physiol. 1984; 247:H909–H915. [PubMed: 6239553]
31. Park CS, Cha H, Kwon EJ, Jeong D, Hajjar RJ, Kranias EG, Cho C, Park WJ, Kim DH. AAV-mediated knock-down of HRC exacerbates transverse aorta constriction-induced heart failure. PLoS One. 2012; 7(8):e43282. [PubMed: 22952658]
32. Piacentino V 3rd, Weber CR, Gaughan JP, Margulies KB, Bers DM, Houser SR. Modulation of contractility in failing human myocytes by reverse-mode Na+/Ca2+ exchange. Ann N Y Acad Sci. 2002; 976:466–471. [PubMed: 12502596]
33. Picello E, Damiani E, Margreth A. Low-affinity Ca^{2+}-binding sites versus Zn^{2+}-binding sites in histidine-rich Ca^{2+}-binding protein of skeletal muscle sarcoplasmic reticulum. Biochem Biophys Res Commun. 1992; 186:659–667. [PubMed: 1497654]
34. Puglisi JL, Bassani RA, Bassani JW, Amin JN, Bers DM. Temperature and relative contributions of Ca^{2+} transport systems in cardiac myocyte relaxation. Am J Physiol. 1996; 270:H1772–H1778. [PubMed: 8928885]
35. Ramirez RJ, Sah R, Liu J, Rose RA, Backx PH. Intracellular [Na^{+}] modulates synergy between Na^{+}/Ca^{2+} exchanger and L-type Ca^{2+} current in cardiac excitation-contraction coupling during action potentials. Basic Res Cardiol. 2011; 106:967–977. [PubMed: 21779914]
36. Ridgeway AG, Petropoulos H, Siu A, Ball JK, Skerjanc IS. Cloning, tissue distribution, subcellular localization and overexpression of murine histidine-rich Ca^{2+} binding protein. FEBS Lett. 1999; 456:399–402. [PubMed: 10462052]
37. Shah AM, Sauer H. Transmitting biological information using oxygen: Reactive oxygen species as signalling molecules in cardiovascular pathophysiology. Cardiovasc Res. 2006; 71:191–194. [PubMed: 16781690]
38. Solaro RJ, Briggs FN. Estimating the functional capabilities of sarcoplasmic reticulum in cardiac muscle. Calcium binding. Circ Res. 1974; 34:531–540. [PubMed: 4826929]
39. Sossalla S, Maurer U, Schotola H, Hartmann N, Didié M, Zimmermann WH, Jacobshagen C, Wagner S, Maier LS. Diastolic dysfunction and arrhythmias caused by overexpression of $CaMKII\delta_C$ can be reversed by inhibition of late Na^{+} current. Basic Res Cardiol. 2011; 106:263–272. [PubMed: 21174213]
40. Terentyev D, Kubalova Z, Valle G, Nori A, Vedamoorthyrao S, Terentyeva R, Viatchenko-Karpinski S, Bers DM, Williams SC, Volpe P, Györke S. Modulation of SR Ca^{2+} release by luminal Ca^{2+} and calsequestrin in cardiac myocytes: effects of CASQ2 mutations linked to sudden cardiac death. Biophys J. 2008; 95:2037–2048. [PubMed: 18469084]
41. Terentyev D, Cala SE, Houle TD, Viatchenko-Karpinski S, Györke I, Terentyeva R, Williams SC, Györke S. Triadin overexpression stimulates excitation-contraction coupling and increases predisposition to cellular arrhythmia in cardiac myocytes. Circ. Res. 2005; 96:651–658. [PubMed: 15731460]
42. Toischer K, Lehnart SE, Tenderich G, Milting H, Körfer R, Schmitto JD, Schöndube FA, Kaneko N, Loughrey CM, Smith GL, Hasenfuss G, Seidler T. K201 improves aspects of the contractile performance of human failing myocardium via reduction in Ca^{2+} leak from the sarcoplasmic reticulum. Basic Res Cardiol. 2010; 105:279–287. [PubMed: 19718543]
43. van Heeswijk MP, Geertsen JA, van Os CH. Kinetic properties of the ATP-dependent Ca^{2+} pump and the Na^{+}/Ca^{2+} exchange system in basolateral membranes from rat kidney cortex. J Membr Biol. 1984; 79:19–31. [PubMed: 6737462]
44. Viatchenko-Karpinski S, Terentyev D, Györke I, Terentyeva R, Volpe P, Priori SG, Napolitano C, Nori A, Williams SC, Györke S. Abnormal calcium signaling and sudden cardiac death associated with mutation of calsequestrin. Circ Res. 2004; 94:471–477. [PubMed: 14715535]
45. Vinet L, Pezet M, Bito V, Briec F, Biesmans L, Rouet-Benzineb P, Gellen B, Prévilon M, Chimenti S, Vilaine JP, Charpentier F, Sipido KR, Mercadier JJ. Cardiac FKBP12.6 overexpression protects against triggered ventricular tachycardia in pressure overloaded mouse hearts. Basic Res Cardiol. 2012; 107:246. [PubMed: 22311731]

46. Wang HS, Cohen IS. Calcium channel heterogeneity in canine left ventricular myocytes. J Physiol. 2003; 547:825–833. [PubMed: 12562927]

47. Wehrens XH. Leaky ryanodine receptors cause delayed afterdepolarizations and ventricular arrhythmias. Eur Heart J. 2007; 28:1054–1056. [PubMed: 17459904]

48. Zhang L, Kelley J, Schmeisser G, Kobayashi YM, Jones LR. Complex formation between junctin, triadin, calsequestrin, and the ryanodine receptor. Proteins of the cardiac junctional sarcoplasmic reticulum membrane. J Biol Chem. 1997; 272:23389–23397. [PubMed: 9287354]

49. Zhao W, Yuan Q, Qian J, Waggoner JR, Pathak A, Chu G, Mitton B, Sun X, Jin J, Braz JC, Hahn HS, Marreez Y, Syed F, Pollesello P, Annila A, Wang HS, Schultz Jel J, Molkentin JD, Liggett SB, Dorn GW 2nd, Kranias EG. The presence of Lys27 instead of Asn27 in human phospholamban promotes sarcoplasmic reticulum Ca^{2+}-ATPase superinhibition and cardiac remodeling. Circulation. 2006; 113:995–1004. [PubMed: 16476846]

50. Zhou X, Fan GC, Ren X, Waggoner JR, Gregory KN, Chen G, Jones WK, Kranias EG. Overexpression of histidine-rich Ca^{2+}-binding protein protects against ischemia/reperfusion-induced cardiac injury. Cardiovasc Res. 2007; 75:487–497. [PubMed: 17499229]

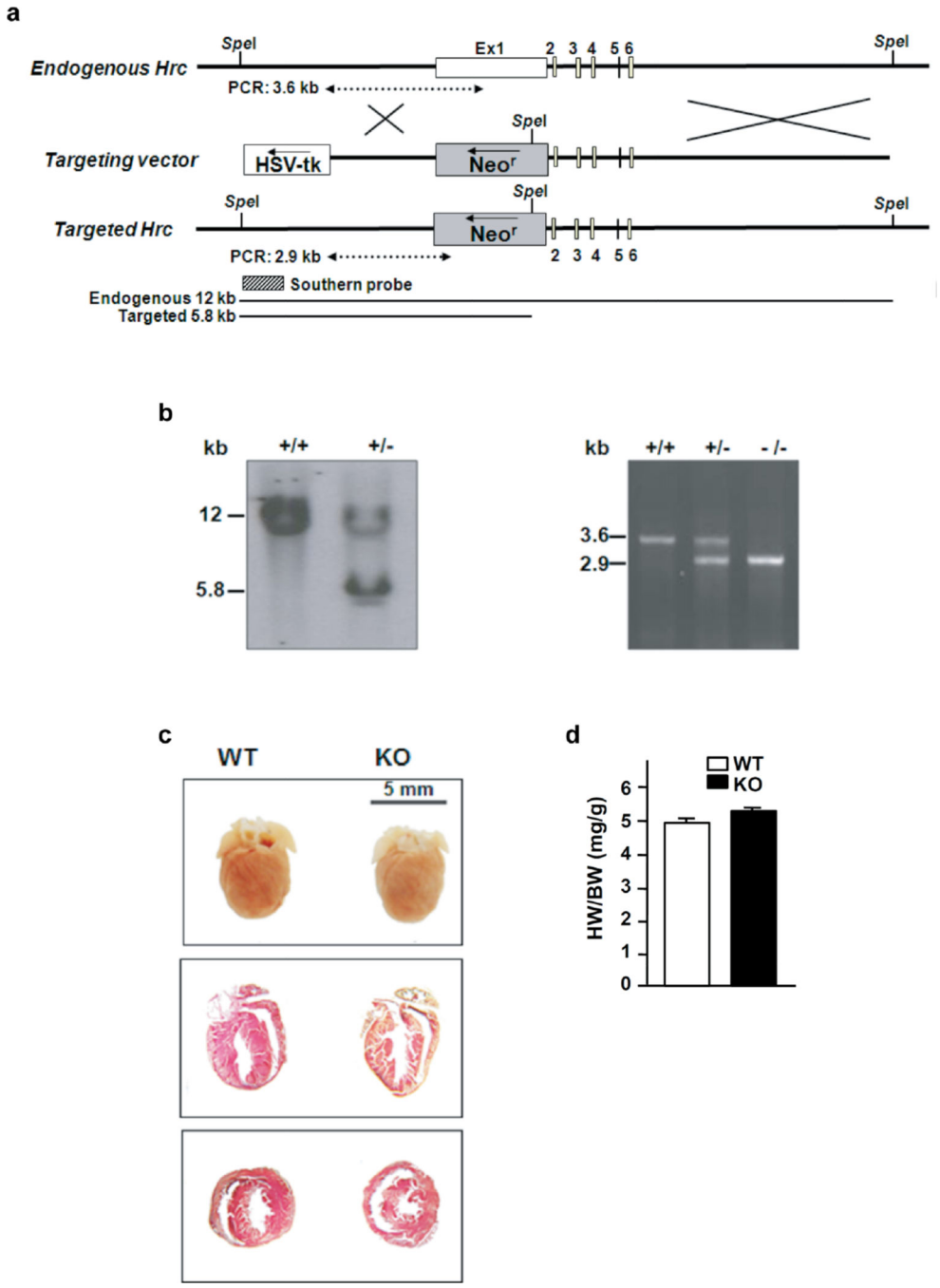

Fig. 1. Targeted disruption of the *Hrc* gene in mice and general cardiac characteristics of hearts lacking HRC

a: Gene targeting strategy. Exons and introns are represented by vertical bars and intervening horizontal lines, respectively. A neomycin-resistance (neo^r) gene driven by a PGK promoter and herpes simplex virus thymidine kinase gene (tk) are indicated as gray and white boxes. b: Left, Southern blot analysis of wild type (+/+) and targeted (+/−) embryonic stem cells (ESC). Genomic DNAs from ESCs were digested with *SpeI* and hybridized with a Southern probe. The wild-type and mutant alleles generated 12 kb and 5.8 kb bands, respectively. Right, allele-specific PCR after extraction of genomic DNA from mice. 3.6- and 2.9-kb products were generated from the wild-type mice and mutant mice, respectively. c: Upper, representative gross morphology of hearts from WT and KO mice. Hearts were longitudinally (middle) or transversely (lower) sectioned and stained

with hematoxylin and eosin. d: Comparison of heart weight to body weight ratio (HW/BW) (n=15 hearts for WT mice and n=12 hearts for KO mice). Data are means ± SEM.

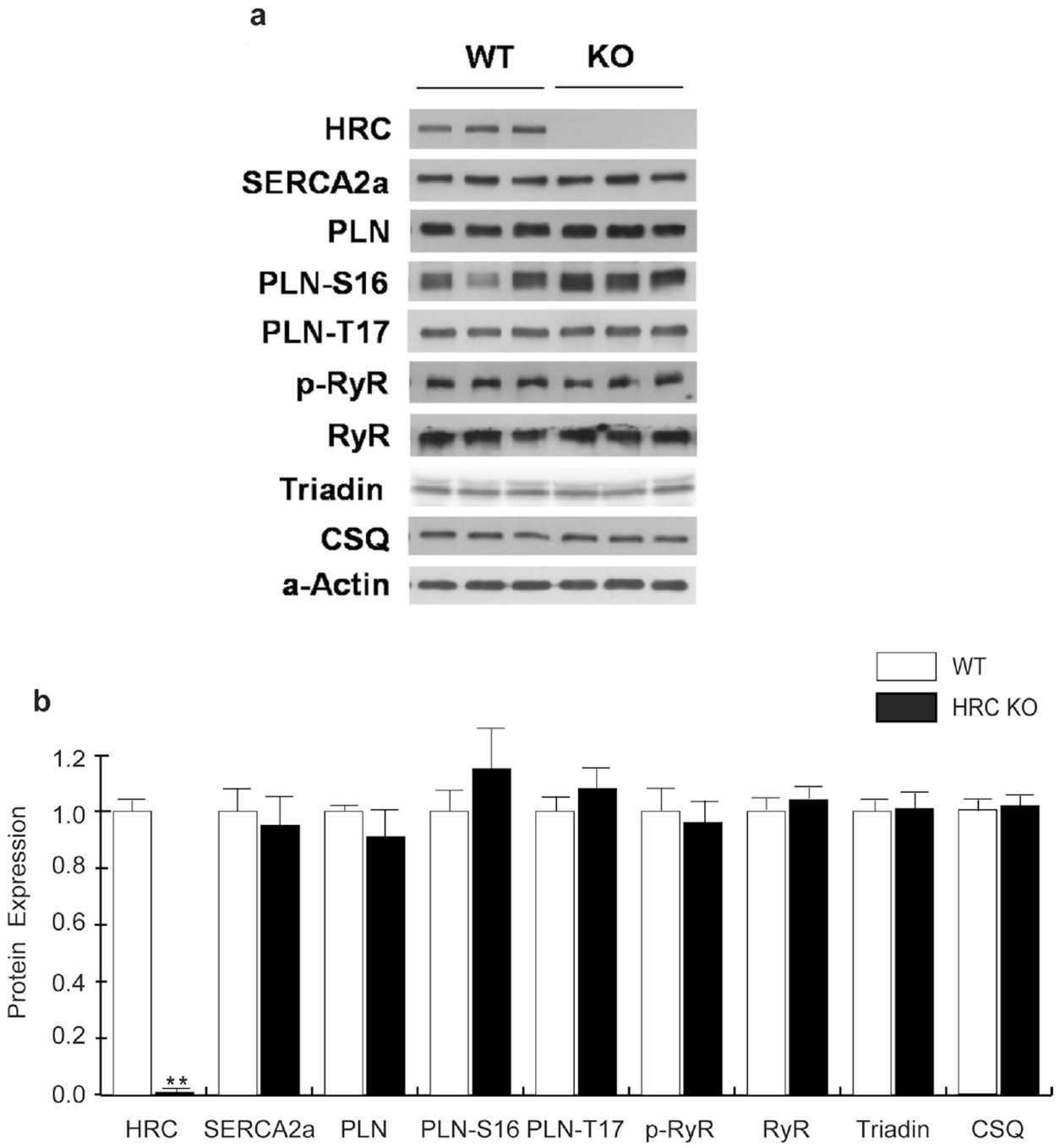

Fig. 2. Immunoblot analysis of Ca^{2+}-cycling proteins from WT and KO mice

Cardiac protein samples were separated by SDS-PAGE and immunoblotting was performed with antibodies against various Ca^{2+}-cycling proteins. a: Representative western blot results of SR Ca^{2+}-cycling protein levels in WT and HRC-KO hearts. b: Quantification of SR protein levels in WT and HRC-KO hearts. p-RyR2 indicates phosphorylated RyR2 at serine 2809 and 2814; PLN, phospholamban; CSQ, calsequestrin. Data are means ± SEM; n=6 hearts for WT or HRC KO mice. *P<0.05.

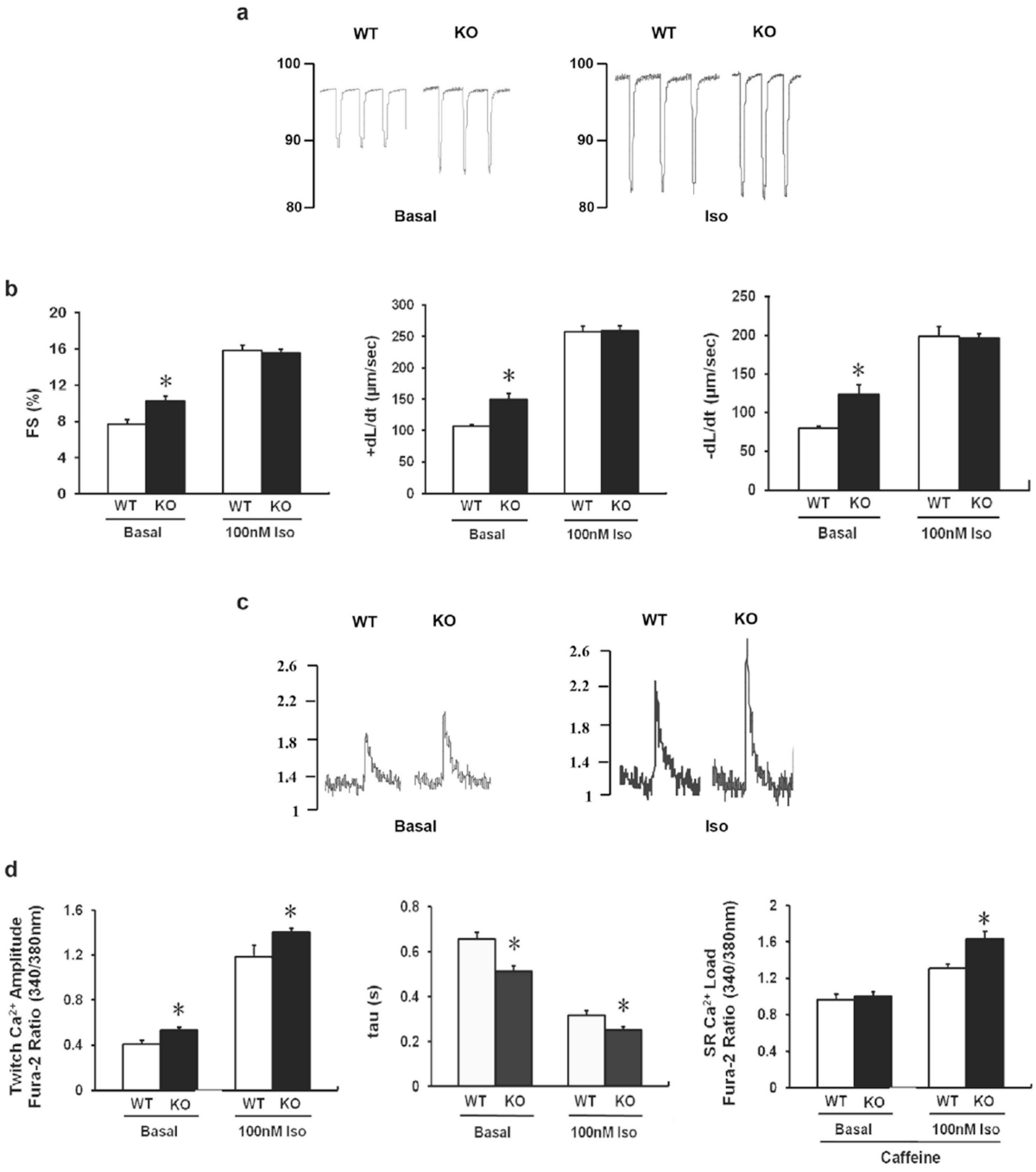

Fig. 3. Mechanics and Ca^{2+} kinetics of HRC-KO myocytes and their response to isoproterenol

a: Representative cell shortening tracings of WT and HRC-KO cells before and after isoproterenol stimulation. b: The fractional shortening and ±dL/dt were measured in the absence and presence of 100nmol/L isoproterenol. c: Representative tracing of Ca^{2+} transients in WT and HRC-KO cells before or after isoproterenol stimulation. d: Amplitude of Ca^{2+} transients, time constant of twitch Ca^{2+} decay (τ) and amplitude of caffeine-induced Ca^{2+} transients were measured in the absence and presence of isoproterenol (100 nmol/L). n=32 cells from 3 WT hearts; n=45 cells from 4 KO hearts; n=23 cells from 3 WT hearts; n=27 cells from 4 KO hearts were used. Data are means ± SEM. *P<0.05.

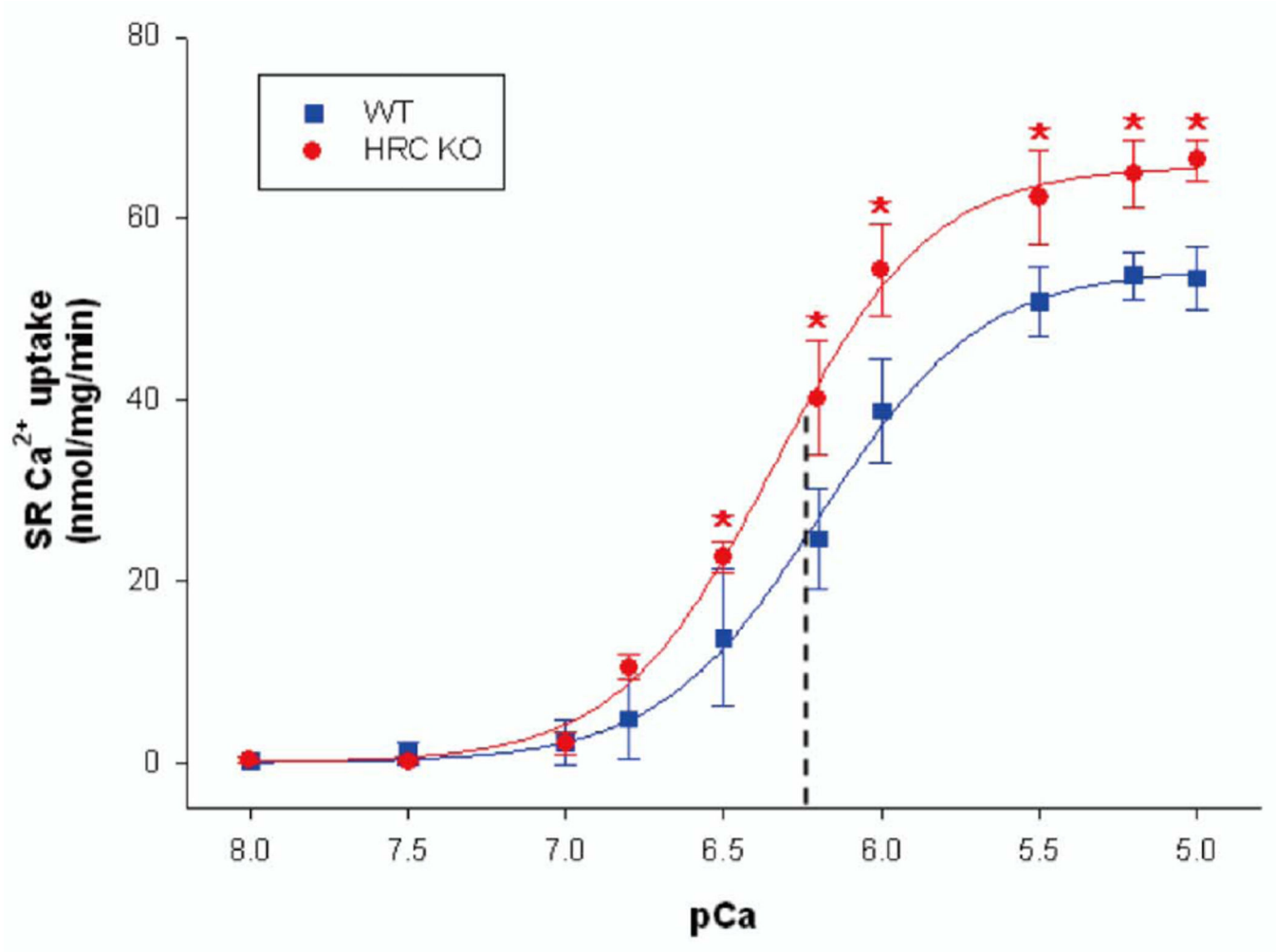

Fig. 4. Ca^{2+}-dependence of oxalate-supported SR Ca^{2+} uptake in WT and HRC-KO mice

The initial rates of SR Ca^{2+} uptake were measured using whole homogenates of WT and HRC-KO mouse heart as described in "Materials and Methods". Vmax, and EC^{50} (dotted line) were calculated by computer fitting. n=3 hearts for WT or HRC KO mice, each assayed in triplicate. Values are mean ± SEM. *P<0.05.

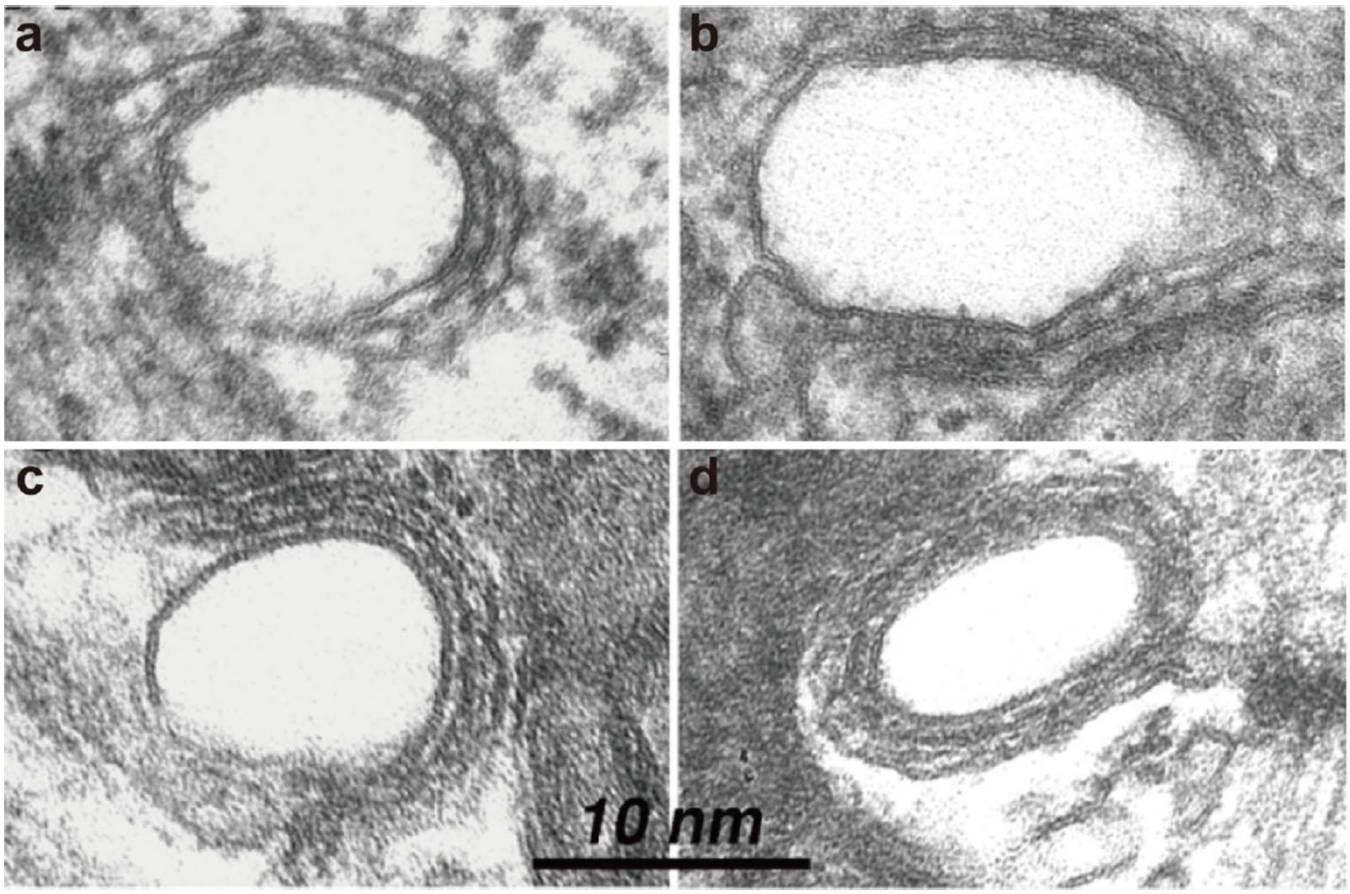

Fig. 5. Electron micrographs from thin sections of papillary muscles from WT (a and b) and HRC-KO hearts (c and d)

The dyadic junctions between the junctional SR (seen as a narrow cisterna with a dense content) and the T tubules (large profiles) are unaltered. RyRs, seen as periodic densities between SR and T tubules, are present at apparently the same frequency in both types of hearts. We found a small (~15%) but statistically significant (Student's *t* test, $P<0.0005$) increase in the overall SR surface area per fiber volume, from 0.28 ± 0.11 $\mu m^2/\mu m^3$ (n=169 fibers from 3 mice) in WT, to 0.33± 0.15 $\mu m^2/\mu m^3$ (n=167 fibers from 3 mice) in HRC-KO cells. The SR volume relative to the fiber volume was not significantly different. V_{SR}/V_{fiber} is 1.68±0.66 (n=172 fibers from 3 mice) in WTs and 1.80±0.71 $\mu m^2/\mu m^3$ (n=166 fibers from 3 mice) in HRC-KOs.

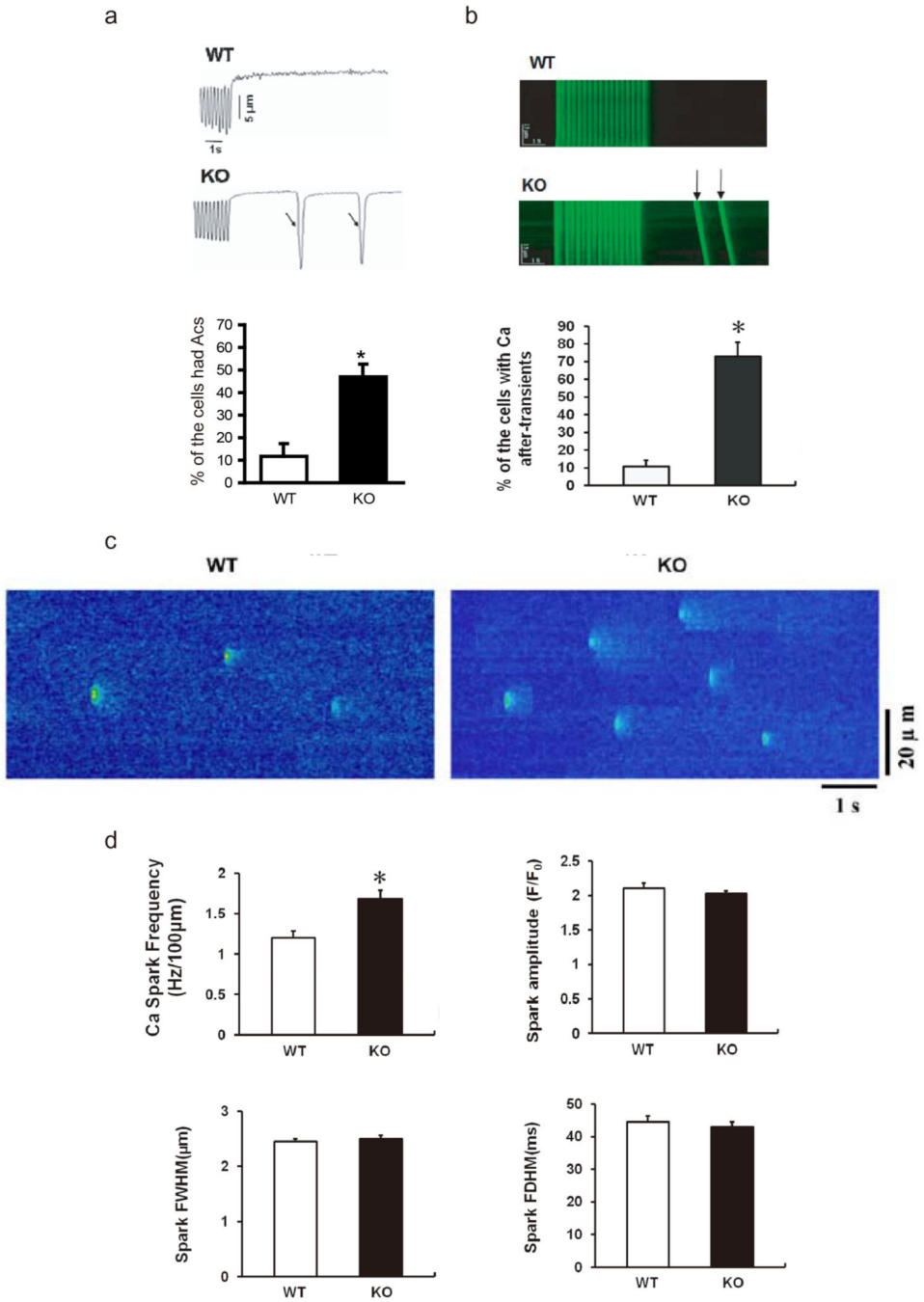

Fig. 6. After-contractions (Acs), spontaneous SR Ca^{2+} release, DADs and Ca^{2+} sparks in HRC-KO ca rdiomyocytes

a: Upper, representative traces of after-contractions (Acs) in WT and HRC-KO myocytes at 5 H z stimulation with 1 μmol/L isoproterenol (room temperature). Lower, percentage of WT and HR C-KO cardiomyocytes that developed Acs (n=29 for 3 WT hearts, n=36 for 4 KO hearts). b: Upper, representative traces of spontaneous SR Ca^{2+} release in WT and HRC-KO cells at 5 Hz stimulation with 1 μmol/L isoproterenol (room temperature). Lower, percentage of cells with spontaneous SR Ca^{2+} release (n=32 for 3 WT hearts; n=31 for 3 KO hearts). c: Upper, representative traces of action potential in WT and HRC-KO cells at 5 Hz stimulation with 1 μmol/L isoproterenol (32C). Lower, percentage of the WT and HRC-KO cells that showed DADs (n=12 cell s for 3 WT hearts; n=12 for 3 KO hearts). D: Upper, representative traces of Ca^{2+} sparks in WT and HRC-KO

cardiomyocytes in the presence of 1 μmol/L isoproterenol. Lower, properties of Ca^{2+} s parks in WT and HRC-KO cardiomyocytes in the presence of 1 μmol/L isoproterenol. n=24 cells from 3 WT hearts; n=32 cells from 3 HRC-KO hearts. Data are presented as mean ± SEM. *P<0.05

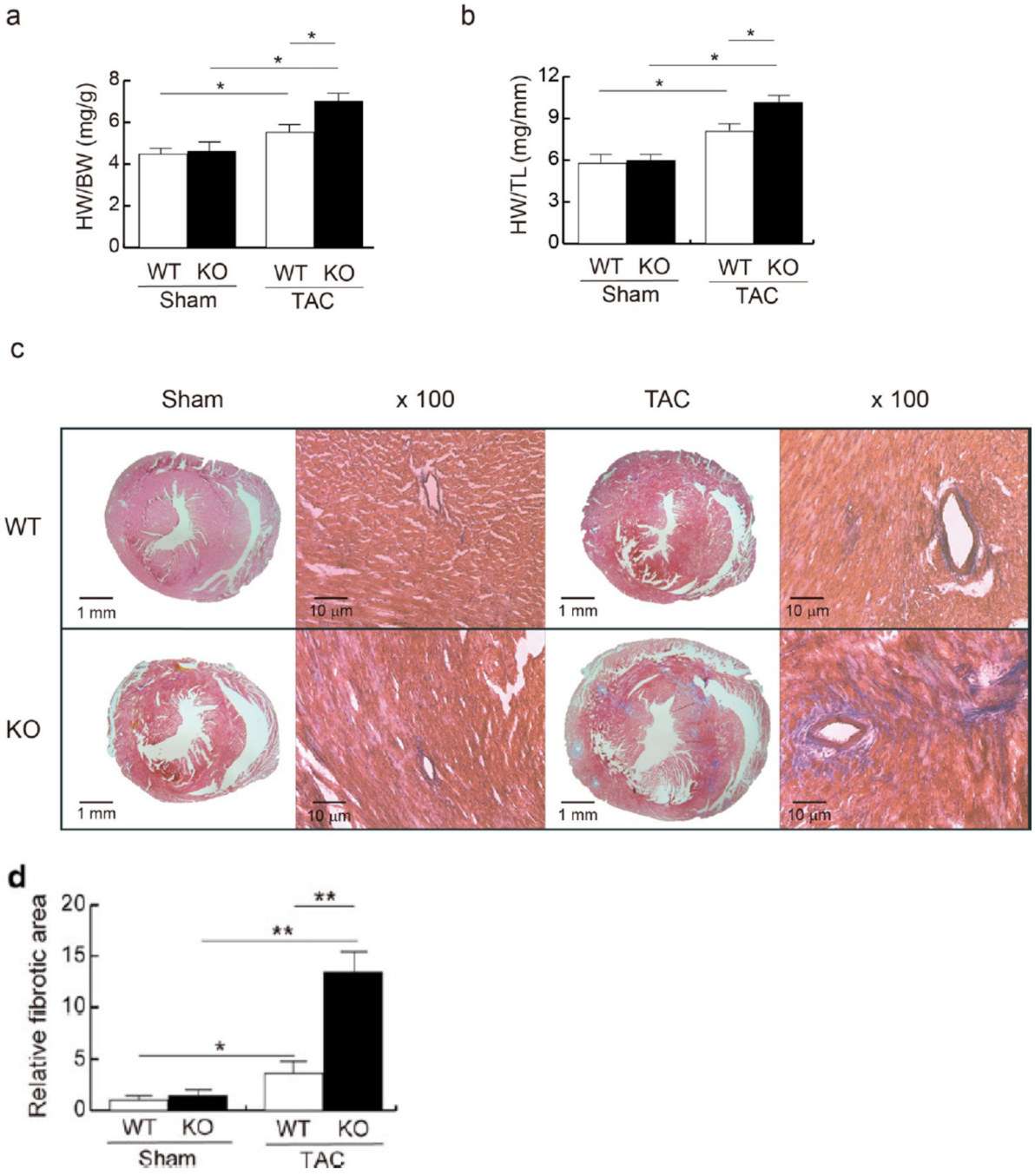

Fig. 7. Increased cardiac hypertrophy and fibrosis in HRC-KO TAC mouse

HW/BW ratio (a) and HW/TL ratio (b) were significantly increased in HRC-KO mice after TAC operation. Masson's trichrome staining results are shown in c. The whole hearts and 100 times magnified images for WT sham and KO sham, and WT TAC and KO TAC are shown. The calculated relative fibrotic areas for each sample are shown in d. The most severe cardiac fibrosis was found in HRC-KO TAC. n=4 hearts from WT sham; n=6 hearts from WT TAC; n=4 hearts from HRC KO sham; n=5 hearts from HRC KO TAC. Data are presented as mean ± SEM. *P<0.05; **P<0.01.

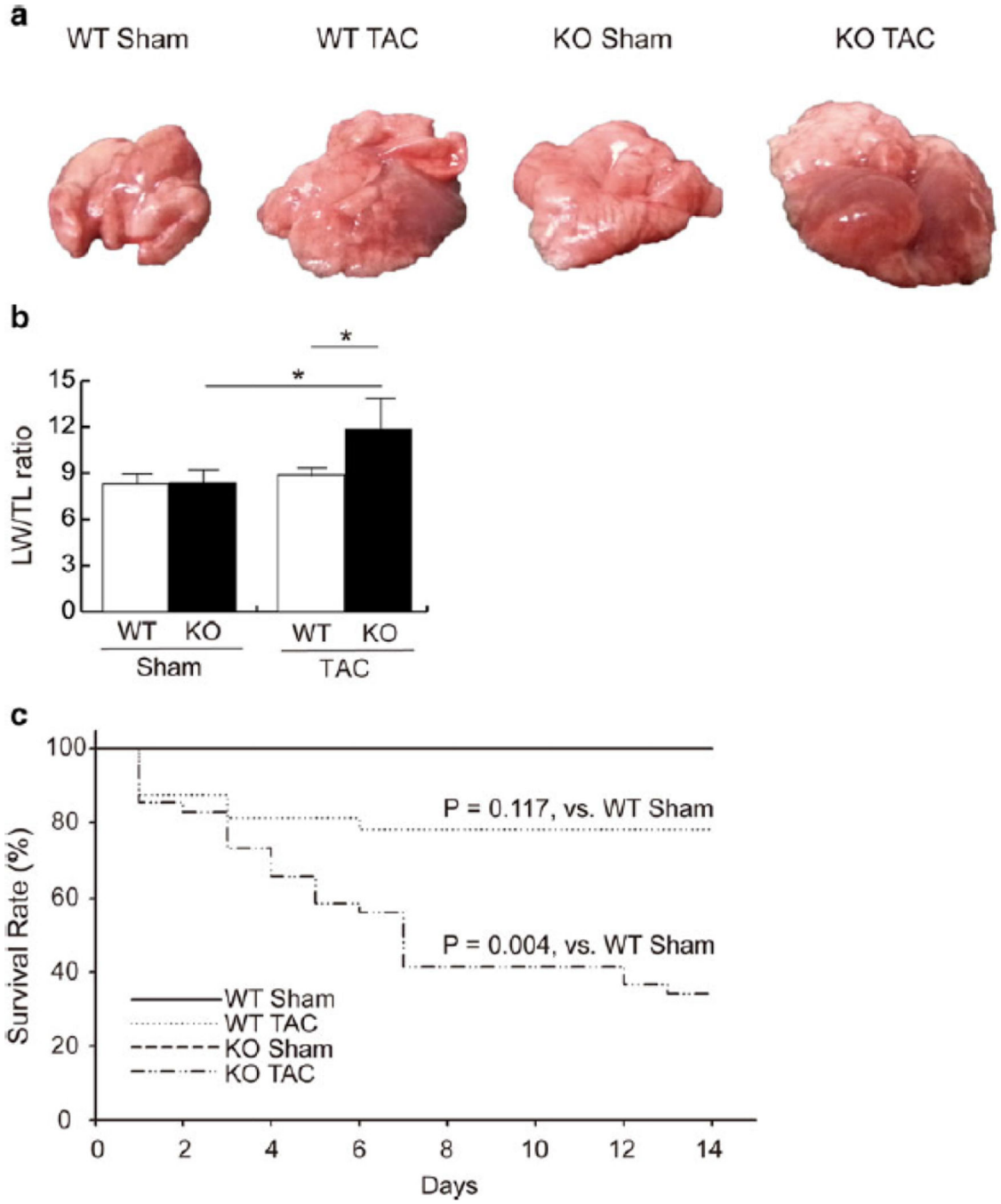

Fig. 8. Severe pulmonary edema and decreased survival rate in HRC-KO TAC animal

a: Representative macroscopic pulmonary changes after sham and TAC operations in WT and HRC-KO mice. Discolored lung and prominent edema were shown in HRC-KO TAC animal. b: The ratio of lung weight over tibia length (LW/TL) was significantly increased in HRC-KO TAC animal. c: Gehan-Breslow analysis for survival rate for the 4 experimental groups is shown. Survival curves of WT sham and KO sham were superimposed. Note that the survival rate of HRC-KO TAC was significantly lower than that of WT-TAC. n=10 mice for WT sham; n=32 mice for WT TAC; n=10 mice for HRC-KO sham; n=41 mice for HRC-KO TAC. *P<0.05.

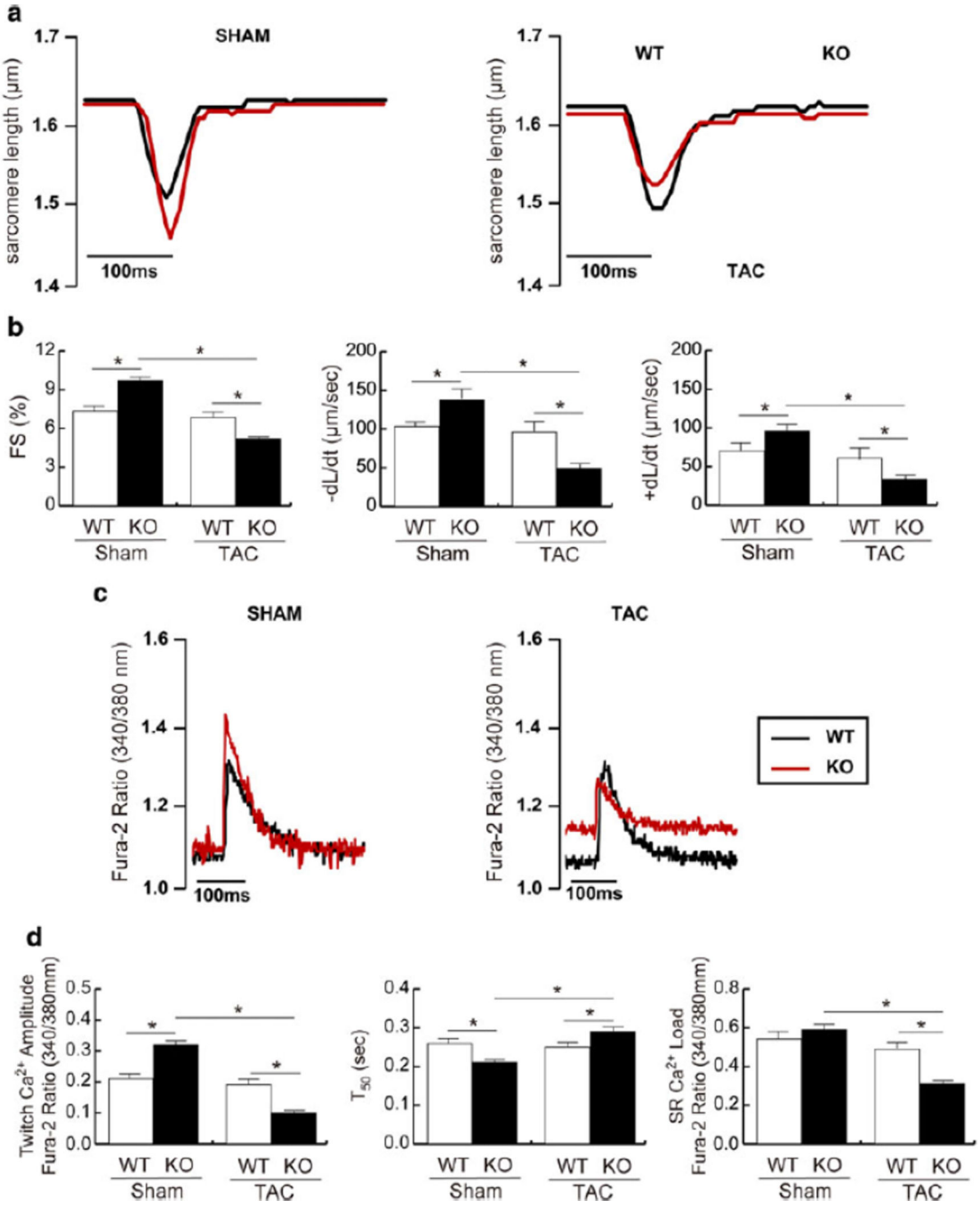

Fig. 9. Mechanics and Ca^{2+} kinetics of HRC-KO myocytes and their responses to pressure over-load

a: Representative cell shortening tracings of WT and HRC-KO cardiomyocytes from sham (left) and TAC (right) groups. b: The fractional shortening and ±dL/dt were measured for the 4 experimental groups (WT/sham, WT/TAC, KO/sham and KO/TAC). c: Representative traces of Ca^{2+} transient in the 4 experimental groups. d: The summary data for amplitude of Ca^{2+} transients, time required to reach 50% of baseline (T^{50}) and amplitude of caffeine-induced Ca^{2+} transients for the 4 experimental groups are shown. n=35 cells from 4 WT sham hearts; n=49 cells from 4 KO sham hearts; n=52 cells from 4 WT TAC hearts; n=58 cells from 4 KO TAC hearts were used. Data are means ± SEM. *P<0.05; **P<0.01.

Table 1

Echocardiographic data for WT and HRC-KO animals 1 week after sham and TAC operations

	WT		HRCKO	
	sham (n=4)	**TAC (n=6)**	**sham (n=4)**	**TAC (n=5)**
SWTd {mm)	0.767 ± 0.033	1.04 ± 0.051*	0.75 ± 0.05	1.26 ± 0.04#,†
LVEDD (mm)	3.0 ± 0.252	3.28 ± 0.12	3.2 ± 0.091	3.56 ± 0.15
PWTd (mm)	0.767 ± 0.088	1.16 ± 0.068*	0.875 ± 0.048	1.48 ± 0.12#,†
SWTs (mm)	1.533 ± 0.12	1.9 ± 0.071*	1.65 ± 0.087	2.08 ± 0.066#
LVESD (mm)	1.1 ± 0.115	1.34 ± 0.087	1.175 ± 0.025	2.12 ± 0.201#,†
PWTs (mm)	1.467 ± 0.088	1.98 ± 0.136*	1.6 ± 0.163	2.16 ± 0.121#
FS (%)	63.413 ± 1.741	59.285 ± 1.416	63.241 ± 0.714	40.916 ± 3.257#,†

SWTd, diastolic septal wall thickness; SWTs, septal wall thickness; LVEDD, LV end-diastolic dimension; LVESD, LV end-systolic dimension; PWTd, diastolic posterior wall thickness; PWTs, systolic posterior wall thickness; FS, fractional shortening. Data are means ± SEM.

*$P < 0.05$ versus WT sham

#$P < 0.05$ versus HRC-KO sham

†$P < 0.05$ versus WT TAC.